



Mapping causal agents of disturbance in boreal and arctic ecosystems of North America using time series of Landsat data

Yingtong Zhang ^{a,*}, Curtis E. Woodcock ^a, Shijuan Chen ^a, Jonathan A. Wang ^{a,b},
Damien Sulla-Menashe ^{a,c}, Zhenpeng Zuo ^a, Pontus Olofsson ^a, Yetianjian Wang ^a, Mark
A. Friedl ^a

^a Department of Earth and Environment, Boston University, Boston, MA, USA

^b Department of Earth System Science, University of California, Irvine, Irvine, CA, USA

^c Indigo Ag, 500 Rutherford Ave suite 201, Boston, MA, USA.

ARTICLE INFO

Editor: Marie Weiss

Keywords:

Time series
Disturbance
Insects
Landsat
ABoVE
Tasseled Cap
Fire
Logging

ABSTRACT

The arctic and boreal biomes are changing as temperatures increase, including changes in the type, frequency, intensity, and seasonality of disturbances. However, our understanding of the frequency, extent, and causes of disturbance events remains incomplete. Disturbances such as fire, forest harvest, drought, wind, flooding, and insects and pathogens occur at different frequencies and severities, posing challenges to characterize and assess them under a single framework. We used the Continuous Change Detection and Classification (CCDC) algorithm on all available Landsat observations from 1984 to 2014 to detect land cover and land condition change. We mapped the following causes of disturbances annually across the study domain of NASA's Arctic Boreal Vulnerability Experiment (ABoVE): fire, logging, and pest damage. Differences between Landsat Tasseled Cap (TC) values pre- and post-disturbance were used in a random forest classifier to map causal agents. For forested ecosystems, we mapped causal agents including *fire*, *insect*, and *logging*. In areas that were not forest before disturbance, only the *fire* class was mapped. The result shows that multidimensional spectral-temporal change information is useful for mapping the causes of disturbance in arctic and boreal biomes. We employed two rounds of post-processing and used the information obtained from the comparison between the map and reference data to improve the final map. The user's and producer's accuracies of an aggregated *disturbance* map were 94.6% (\pm 2.37%) and 89.3% (\pm 21.78%) (95% confidence intervals in parenthesis). When evaluating the causal agents, insect damage was found the most challenging to map and validate. We estimated that 10.8% of the ABoVE core domain was disturbed between 1987 and 2012, with a margin of error of 0.5% at the 95% confidence level. Rates of disturbance due to logging remained constant over time, while fires were more episodic, and insect damage was highest between 2005 and 2010. Overall, fires affected 8.8% of the study area, while logging was 1.4% and insect damage 0.6%. Our maps indicate that pest damage became a significant issue after 2000, but it was more severe for forest ecosystems in Western Canada than in Alaska.

1. Introduction

Arctic and boreal domains are undergoing significant land surface changes in response to rapid climate warming (Alcaraz-Segura et al., 2010; Bonan, 2008; Lawrence and Chase, 2010; Wang et al., 2020). Over the last four decades, the boreal biome has experienced extensive tree canopy loss due to multiple kinds of forest disturbance, and transitions caused by their subsequent recovery (Hermosilla et al., 2019; Song et al., 2018). At the same time, it has been observed that vegetation species

changes are ongoing in Northern Canada and Alaska, and high-latitude forests are projected to expand northward with increasing temperature, which will affect arctic terrestrial ecosystems and may eventually replace the original tundra (Bhatt et al., 2010; Chapin et al., 2005; de Wit et al., 2014; Swann et al., 2010). This trend will bring more disturbances such as wildfire, wind, insect damage, and other forest-related changes, resulting in a positive feedback to further warm the Arctic (Overpeck et al., 1990; Price et al., 2013; Seidl et al., 2017). Monitoring northern high latitude disturbances is pivotal, given not only their

* Corresponding author at: 675 Commonwealth Ave., Boston University, Boston, MA 02215, USA.

E-mail address: zhangyt@bu.edu (Y. Zhang).

effects on ecological functions and impacts on surrounding ecosystems and wildlife but also the need to estimate carbon fluxes, especially considering the immense and vulnerable stores of carbon in arctic and boreal soils (Hugelius et al., 2014). One of the key questions in NASA's Arctic-Boreal Vulnerability Experiment (ABoVE) concerns the kinds, patterns, and frequencies of land surface changes and ecosystem dynamics over the past 25–50 years (Fisher et al., 2018; Kasischke et al., 2010a). One remaining gap in our understanding of land change in boreal and arctic environments is the spatial and temporal patterns of the primary disturbances at spatial resolutions that capture landscape patterns.

It is challenging to map the causal agents of ecosystem disturbances, especially over regional to global scales at a high spatial and temporal frequency (Wulder et al., 2004). Usually, disturbance studies only consider a single agent, which makes comprehensive analyses of disturbance agents harder. Fire has been well-studied from the perspectives of occurrence, severity, and post-disturbance ecological functionality (Bond-Lamberty et al., 2007; French et al., 2008; Johnstone et al., 2010; Kasischke et al., 2010b; Loboda et al., 2018; Tyukavina et al., 2017). However, pest damage has rarely been characterized over a continental scale, though some case studies investigated it at a regional scale (Bright et al., 2020; Burton and Boulanger, 2018; Franklin and Robitaille, 2020; Turner et al., 2015). Satellite remote sensing data are key to characterizing disturbance across continents and decades, but this application has historically been limited by several challenges, including the ability to maintain and process large volumes of data; obtaining anniversary date images for disturbance mapping due to the limited availability of clear observations before and after disturbances; the difficulty of finding suitable models for time series data analysis; and questions concerning how to compare results with existing products when they are based on different temporal/spatial resolutions (Ju and Roy, 2008; Wulder et al., 2012; Zhu, 2017).

Since open-access to the Landsat archive in 2008, the approaches for analysis of Landsat data for change detection have progressed remarkably (Loveland and Dwyer, 2012; Woodcock et al., 2008). Access to all available 30-m spatial resolution observations from Landsat provided new opportunities to investigate long-term land cover change and led to a number of approaches based on time series, such as LandTrendr (Kennedy et al., 2010), Vegetation Change Tracker (VCT, Huang et al., 2010), Breaks For Additive Seasonal and Trend (BFAST, Verbesselt et al., 2010), Continuous Change Detection and Classification (CCDC, Zhu and Woodcock, 2014a), and Composite2Change (C2C, Hermosilla et al., 2016). VCT, LandTrendr, and C2C are trajectory-based change detection algorithms applied to annual image stacks that rely on the availability of enough images to provide a cloud-free composite image for each year. These algorithms have been used extensively, and recently LandTrendr has been shown to be suitable for both abrupt and gradual change detection (Cohen et al., 2018; Li et al., 2009a, 2009b; Zhao et al., 2015). CCDC, on the other hand, uses all available images and provides predicted values that can be used for both change detection at any desired time scale and near-real-time monitoring (Arévalo et al., 2020b; Pasquarella et al., 2017; Tang et al., 2019). By exploring Landsat-derived NDVI time-series trends and the disturbance datasets, it is also feasible to study the drivers (i.e., climate variables, post-disturbance recovery) of the greening and browning trends observed in high latitude regions (Ju and Masek, 2016; Sulla-Menashe et al., 2018). With the increasing needs and popularity of time series approaches for monitoring change, the CCDC and LandTrendr algorithms are now supported on Google Earth Engine (Kennedy et al., 2018; Gorelick et al., in preparation). A series of tools became available online soon afterwards, designed to support the broader use of CCDC for environmental monitoring (Arévalo et al., 2020a).

Attempts to map the causal agents of disturbance are becoming more common, with the area, severity, and frequency of disturbances taken into account (Curtis et al., 2018; Espírito-Santo et al., 2014; Hermosilla et al., 2019; Schroeder et al., 2017; Senf and Seidl, 2021; Soverel et al.,

2010). The spectral indices commonly used for change detection include Normalized Differential Vegetation Index (NDVI, Tucker, 1979), Normalized Differential Water Index (NDWI, Gao, 1996), Normalized Burn Ratio (NBR, Key and Benson, 2003), Disturbance Index (DI, Healey et al., 2005), and the Tasseled Cap (TC, Crist and Cicone, 1984) indices of Brightness, Greenness, and Wetness. NBR and the change in NBR, or dNBR (Miller and Thode, 2007), are often used for mapping fire/burn severity and harvesting in a variety of ecosystems (Frazier et al., 2018; Meigs et al., 2011; Schroeder et al., 2014; White et al., 2017). The spectral change of areas disturbed by insect damage is more gradual and subtle, making it difficult to detect compared to fire and forest clear-cuts (Hlásny et al., 2021; Senf et al., 2017b). Though differencing single indices like NBR or dNBR is the most frequently used approach in change detection, it is not always sensitive to the gradual changes resulting from insect outbreaks. One alternative is to use the Tasseled Cap (TC) indices of brightness (B), greenness (G), and wetness (W), which have been used to characterize disturbance events that are related to vegetation dynamics and, most frequently, forest-related changes (Cohen et al., 1995; Collins and Woodcock, 1996; Frazier et al., 2015; Masek et al., 2008; Senf et al., 2017a). Healey et al. (2005) tested Tasseled Cap-derived transformations, including BGW, BG, W, and Disturbance Index (DI) against the original Landsat TM data, and found that TC BGW and DI performed the best for detecting forest disturbances. Pasquarella et al. (2017) used the TC Greenness and synthetic images from the Landsat time series to identify defoliation events caused by gypsy moths in near-real-time.

One prominent disturbance product for high latitudes is the forest disturbance dataset produced by the Canadian Forest Service for all of Canada (White et al., 2017). Using the Composite2Change (C2C) algorithm, White et al. (2017) developed an annual forest disturbance and recovery dataset using Landsat time series, where they found the vegetation recovered more rapidly after fires than after harvests, with the recovery rate varying by the magnitude of the disturbance and ecozone. Later, in 2020, the same group published their non-stand replacing (NSR) disturbance products, which are more related to drought stress or insect infestation (Coops et al., 2020). Due to the complexity of training an algorithm and collecting reliable reference data for subtle changes, NSR pixels were not assigned a causal agent, with only the accuracy of the entire NSR disturbance class evaluated. Lately, the CCDC algorithm has been used to produce disturbance products, land cover, and land cover change maps in Arctic Boreal Region from all available Landsat data from 1984 to 2014 (Sulla-Menashe et al., 2016; Wang et al., 2020). The results indicate evergreen forest loss and deciduous forest gain caused by disturbance events. In this paper, we map the drivers of disturbance in the ABoVE study region over three decades for three causal agents: fire, logging, and pest damage. New disturbance datasets with causal agents will provide a more comprehensive level of understanding of changes in the landscape. Also, ecosystem response to climate change with respect to greening/browning can be parsed by excluding disturbance, as climate-induced long-term trends can be confused by harvesting and fire (Sulla-Menashe et al., 2018; Wang et al., 2020).

The main objectives of this effort were to: (1) map disturbances across the study area at an annual time step; (2) map the causal agents of the disturbances as *fire*, *insect*, and *logging*; and (3) assess the accuracy of these maps and estimate the areas (including estimates of uncertainty) of the various kinds of disturbance. In this study, we define "disturbance" as including: (1) events that caused places to change from a forest to a non-forest land cover; and (2) areas other than forests that were burned in a fire. For disturbances in forests, we attempted to identify the cause of the disturbance as *fire*, *insect*, or *logging* (which includes road building).

Additionally, we created a number of other map products that are intended to be helpful to the scientific community, but are difficult, if not impossible to rigorously validate. These include "synthetic reflectance" images, or predicted images of surface reflectance through time,

and annual maps of changes in ecosystem condition, as indicated by changes in TC greenness and wetness. Some types of disturbance not included in our study (e.g., wind, drought, permafrost degradation, lake drainage, etc.) may be found in these changes in Tasseled Cap greenness and wetness.

2. Datasets and methodology

2.1. Study area

Our study area is the ABoVE Core Domain (Loboda et al., 2019) which covers most of Alaska, USA and the Western Provinces of Canada. As a large and complex study area, the ABoVE domain crosses ten Level-I ecological regions, and is mostly covered by tundra, taiga, and boreal forest (Fisher et al., 2018; Wang et al., 2020). The forest composition in Alaska and Western Canada changes with the climate and topography, ranging from boreal forest in arctic areas, to temperate rain forest along the western coast. The most common species include mountain hemlock, white spruce, quaking aspen, paper birch, lodgepole pine, Rocky Mountain fir, black spruce, and tamarack in forested wetlands, and balsam poplar on floodplains (United States Department of Agriculture, 2009). Fire is regarded as the primary cause of boreal forest loss ([datasets] Canadian Council of Forest Ministers, 2019). Still, according to the inventory data from Natural Resources Canada, insect damage is becoming more severe, affecting up to $1.76 \times 10^5 \text{ km}^2$ of Canada's forest, or 12 times the fire-induced forest loss in 2015 (Natural Resources Canada, 2017). Harvesting activities include both selective logging and clear-cutting. Also associated with harvest are new roads, which are often narrow and hard to detect and tend to be ignored when estimating forest loss.

2.2. Landsat data processing

2.2.1. Landsat time series data processing

All available Landsat Thematic Mapper (TM) and Enhanced Thematic Mapper (ETM+) data for the ABoVE core domain were acquired from 1984 to 2014 from the United States Geological Survey (USGS) archive. Function of mask (Fmask) was used to remove clouds, cloud shadows and snow (Zhu and Woodcock, 2014b). Only data from the growing season (June to August) were included, as many areas in winter are covered with snow. The original data in the Landsat WRS2 Path/Row convention was re-tiled and re-projected to the ABoVE standard Reference Grid System and Canadian Albers Equal Area projection for the ABoVE core domain (Loboda et al., 2019), which includes 164 tiles, each

with $6000 \times 6000 30 \text{ m pixels}$ (Fig. 1). There is substantial overlap of Landsat paths at high latitudes, and tiling the data accumulates all the possible observations through time for each pixel. All Landsat spectral bands except the thermal were included.

The CCDC algorithm is “online”, meaning it starts at the beginning of the time series and processes observations sequentially (Zhu and Woodcock, 2014a). Once there are enough observations, a harmonic regression model is fit. With a time series model in place, future observations are predicted using the coefficients for the harmonic regression model. If future observations differ consistently from those predicted (5 consecutive observations outside a threshold of 3 times the RMSE of the time series model), a “break” is established, and a new time series model is fit to future observations. In this way, CCDC divides the time series for each pixel in the study area into a series of “breaks” and “segments”, with segments being defined as the time between breaks. We fit harmonic regressions to each band using three harmonics. While there is a separate model fit for each band, multiple bands (a parameter) are used in determining breaks. In this application, we used the green, red, NIR, and both SWIR bands. We initially tested 40 tiles (164 in total) using a very conservative change threshold of 4.5. However, we found many omission errors for disturbance and very few spurious breaks. To be less conservative and to minimize the errors of omission, we lowered the threshold for detecting a break from 4.5 to 3.5.

“Synthetic images” can be generated using the predicted Landsat surface reflectance for any desired date (Zhu et al., 2015). For land cover mapping, the unit of classification is a segment. Fig. 2, for instance, shows time series plots of three pixels that were disturbed in 2007, the CCDC time series models and breaks that were identified, and the land cover outcomes. Using this approach, a land cover map can be produced at any time covered by the time series. After classifying each time segment, if the land cover is the same for consecutive time segments, the break between those two segments is ignored for the purposes of land cover mapping. Thus, all land cover changes occur at model breaks found by CCDC, but not all breaks are land cover changes.

Most uses of CCDC have been based on the time segments because the coefficients from the model fits and derived spectral-temporal features for each time segment can be useful for land cover classification (Pasquarella et al., 2018). In this study, we focus on the breaks between segments, since these breaks may represent ecosystem disturbances with the magnitude of the breaks being valuable for characterizing disturbance. We fit harmonic regression models using the CCDC algorithm (Holden, 2017; Zhu and Woodcock, 2014a) to Landsat time series from 1984 to 2014 for each pixel, and all pixels with at least one break are identified as possible candidates for the disturbance map. Given that the

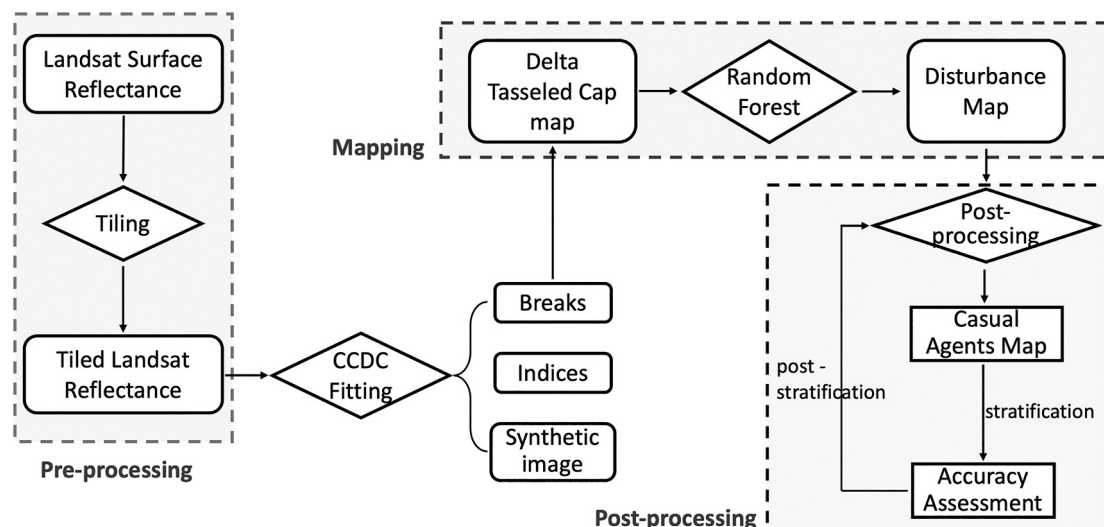


Fig. 1. A schematic representation of the steps used to map disturbance agents.

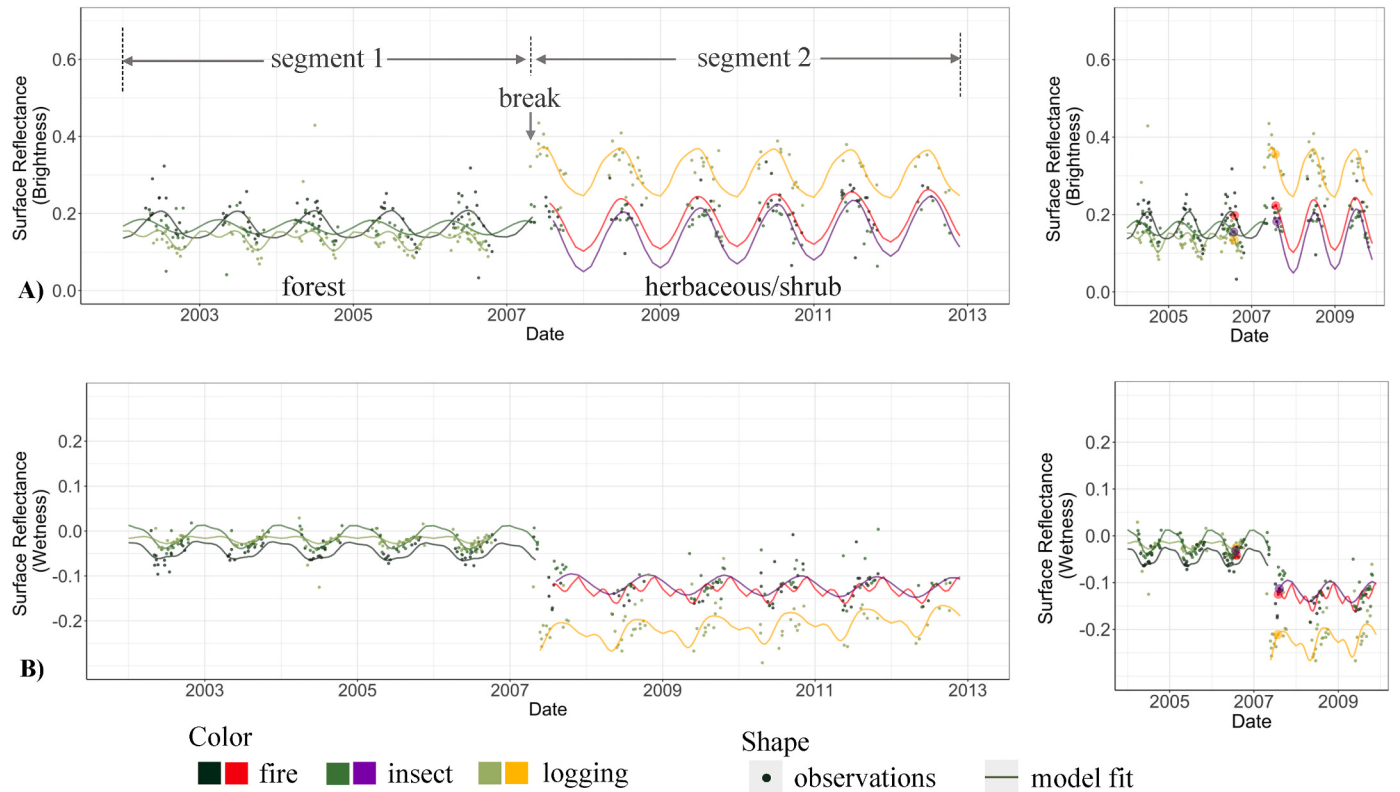


Fig. 2. Landsat time series for three pixels from 2002 to 2013. The left panel includes the entire time series and the right panel is an enlargement around the break points ranging from 2004 to 2011, with the peak summer (Day 212) synthetic values highlighted that were used to calculate ΔTC . Green dots from dark to light represent the Tasseled Cap A) brightness and B) wetness calculated directly from Landsat observations. Curves are model fits which included two “segments” separated by a “break” detected by CCDC in 2007. Three disturbance causal agents are shown for areas that started as the forest and ended as herbaceous or shrubs after experiencing fire, insect damage, or logging. (For interpretation of the references to colour in this figure legend, the reader is referred to the web version of this article.)

CCDC harmonic model is susceptible to commission errors during the beginning years and omission errors at the end of a time series, the time series model was fit from 1984 to 2014 but the final disturbance map was reduced to 1987 to 2012. Since many fewer available Landsat observations were recorded in Alaska before 2000, the Alaska disturbance agents were mapped from 2000 to 2012 and the rest of the domain from 1987 to 2012.

In this study, disturbance indicated all kinds of forest loss (land cover conversion from a forest land cover to non-forest land cover) and fire in non-forest land covers. Note that disturbances are a subset of the breaks found by CCDC. Many things can cause breaks in time series models in CCDC, including climatic variability, repeated clouds missed during the screening process, or other changes in land condition. Hence, the mapping of disturbances can be thought of as a filtering or sorting process: first, sorting the breaks into those that constitute disturbance, and then sorting the breaks associated with disturbance according to their causes.

One of the inputs for the filtering step was a land cover map classified from the CCDC-defined segments from 1984 to 2014 in the ABoVE Core Study Domain (Wang et al., 2020). Evergreen forest, deciduous forest, and mixed forest were combined into a general “forest” class for the entire core region, with all other vegetated classes and barren combined into a “non-forest” class. By aggregating the initial 15-class land cover map into two simpler classes, we improved the accuracy of the map and simplified the question of where forest land covers had been converted to non-forest, as according to our definition, all areas converted from forest to non-forest land covers were considered disturbance. The overall accuracy of the map (Wang et al., 2020) following aggregation was $91.5\% \pm 0.26$. Its accuracy is critical because it is used in the sorting of breaks.

2.3. Mapping causal agents of disturbance

2.3.1. Derivation of ΔTC and the spectral-temporal signature of causal agents of disturbance

In a similar way that the coefficients from harmonic models fit to time segments have been utilized for mapping land covers (Wang et al., 2020), the spectral-temporal features associated with CCDC model breaks can be used to differentiate kinds of land change. Specifically, we used the three TC indices, brightness, greenness, and wetness (B, G, and W) and the change in B, G, and W (ΔB , ΔG , and ΔW) following breaks to classify the causal agents of disturbance. Differences in the TC indices were calculated from the peak summer reflectance values, defined as day 212, for the year before and the year after the CCDC model breaks to minimize complications related to the timing of disturbances:

$$\Delta TC[i, t] = TC_a[i, t] - TC_b[i, t - 1] \quad (1)$$

where TC_a is a vector of B, G, and W values after the break in the model of pixel i in year t , and TC_b corresponds to the values for peak summer from the year before the break. If the disturbance happens before peak summer in a given year, it will be included in the maps associated with that year. Otherwise, the disturbance will be included in the disturbance map of the next year.

The ΔTC images shown in Fig. 3 illustrate the spectral differences for the various change agents in the three components. Across the top of Fig. 3 (panels 3a, 3b, and 3c) are synthetic images at three times for the same location. Colour composites of images of ΔB , ΔG , and ΔW across the bottom for the same location for the same three times (panels 3d, 3e, and 3f) show the pixels where a break was found by CCDC for the years indicated, otherwise they remain white. A fire occurred in 1991, within

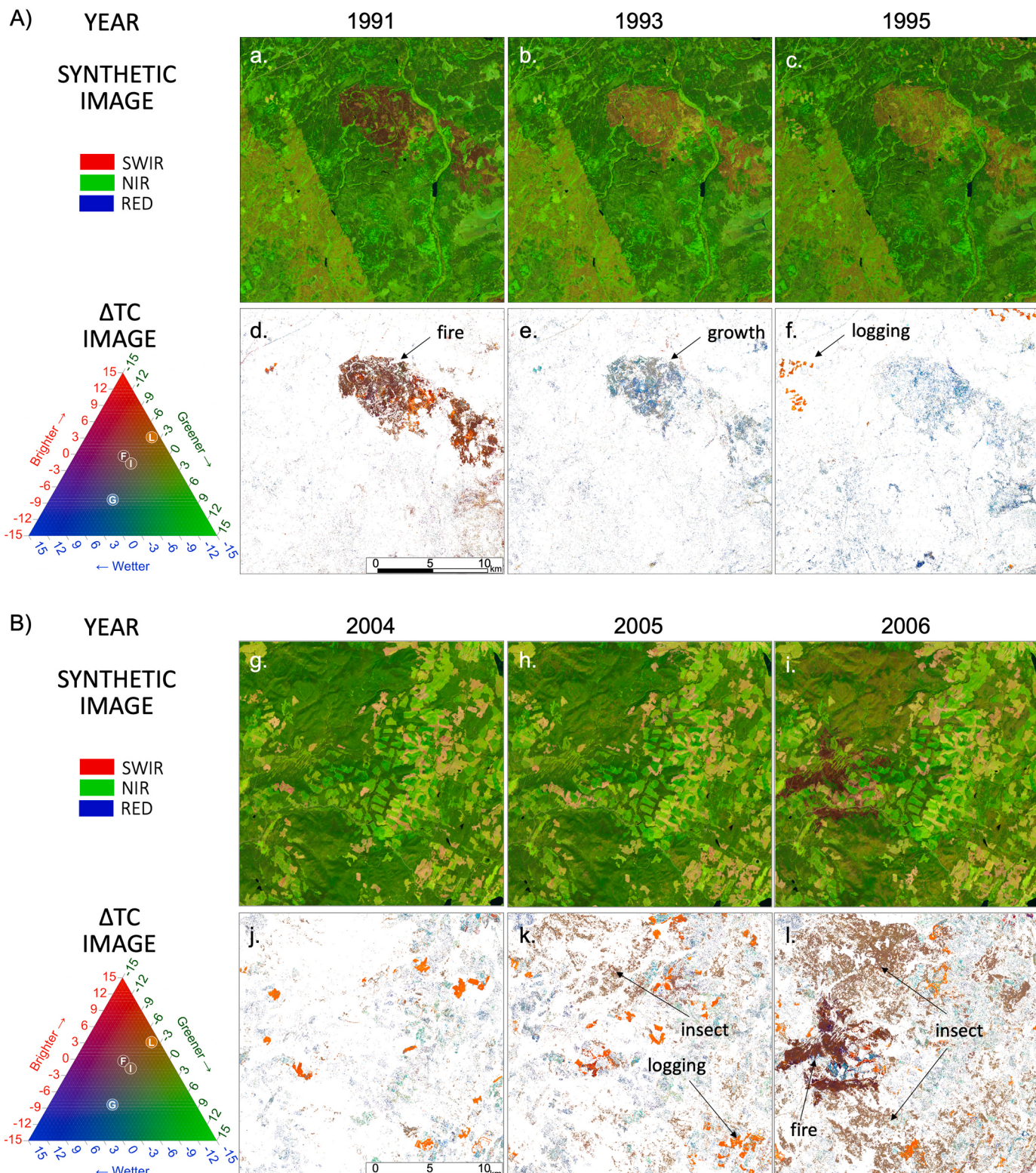


Fig. 3. The outputs of CCDC for two regions. A) Panels a, b, and c are synthetic images during the same year as a fire (1991), two (1993), and four years (1995) post-fire. b) Panels g, h, and i are synthetic images in the year before (2004) and experiencing the pest damage (2005, 2006). RGB combinations of synthetic images are the SWIR, NIR, and Red bands stretched from 0 to 0.4. Panels d, e, f, j, k, and l are Δ Tasseled Cap images in corresponding years. Where there is a model break, the values correspond to the change in BGW before and after the break. Pixels without a break are left in white. The ternary legend includes examples of RGB combinations of fire (F), insect (I), logging (L), and post-disturbance growth (G) signals, and the label was rescaled by dividing 100. (For interpretation of the references to colour in this figure legend, the reader is referred to the web version of this article.)

which there are several areas of salvage logging. In the later panels, vegetation recovery is evident. The ΔTC components in general have different signals for the different causal agents across the study domain. In these composites, fires are mostly maroon or dark browns, corresponding to less bright, less green, and less wet. Insect damage is light brown, similar to the low severity fire but more scattered spatially. Logging patches appear orange and have the opposite spectral signal in brightness compared to fire, due to the exposed bare ground after tree loss. However, sometimes logged areas can become greener due to the replacement of evergreen trees with grasses and broadleaf species that have a “greener” spectral signature. Other ΔTC combinations indicate more complicated land condition changes. One apparent pattern is that the cyan colour (increases in G and W) is indicative of post-disturbance recovery of vegetation.

2.3.2. ΔTC and change agent attribution

We used the aggregated land cover change maps from Wang et al. (2020) (ABoVE land cover map) to guide the process of identifying training data and exploring the relationship between ΔTC and the different types of disturbance. After the ABoVE land cover map was simplified to forest (F) and non-forest (N), land cover change was defined as a change between those two simple categories. Fig. 4 describes how the detected breaks were attributed and switched to other classes within Forest-to-Forest (FF), Forest-to-Nonforest (FN), Nonforest-to-Forest (NF), and Nonforest-to-Nonforest (NN) categories at the pixel scale after classification, automatic post-processing, and rule-based post-processing procedures.

First, breaks associated with places that had remained forest in

ABoVE land cover map, or FF, were sorted into “FF growth” and “FF decline” based on their ΔTC values (Fig. 4). Forest growth (FF growth) is easy to identify as it leads to increases in G and W. FF decline was identified as areas that did not change land cover but decreased in G and W. Areas that changed from non-forest vegetation to forests (NF) in the land cover map were considered to have increased in vegetation and were not considered for disturbance. “NNother” are breaks that were not further categorized but had changes in W and G. We randomly sampled 100 pixels with very low magnitudes ΔTC values from the FF, NF, and NNother populations and visually interpreted them. The interpretation result shows that when ΔTC values are below 0.002, the break is likely to be noise rather than indicative of disturbance. Therefore, an empirical threshold was set to remove very low magnitude breaks in an attempt to avoid errors of commission in the disturbance maps.

Second, all the breaks that changed from forest to non-forest (FN) and non-forest to non-forest (NN, includes NNfire and NNother) were classified into six categories using a random forest classifier in R (Breiman, 2001; Liaw and Wiener, 2002), including four FN categories and two NN groups (Fig. 4). The four FN categories were initially designed to include all kinds of causalities of disturbance, where *other* was targeted to capture all the other types of disturbance except for *fire*, *logging*, or *insect*, which possibly includes drought, wind, flooding, and others. However, given the challenges associated with defining the *other* class and the difficulty for assessing its accuracy, we decided to only map and rigorously validate the causal agents of *fire*, *logging*, or *insect* in our final results. A more detailed version of Fig. 4 is shown in the supplementary material (Fig. s1), including the population of pixels that changed from categories in ΔTC images to the sorted disturbance agents and land

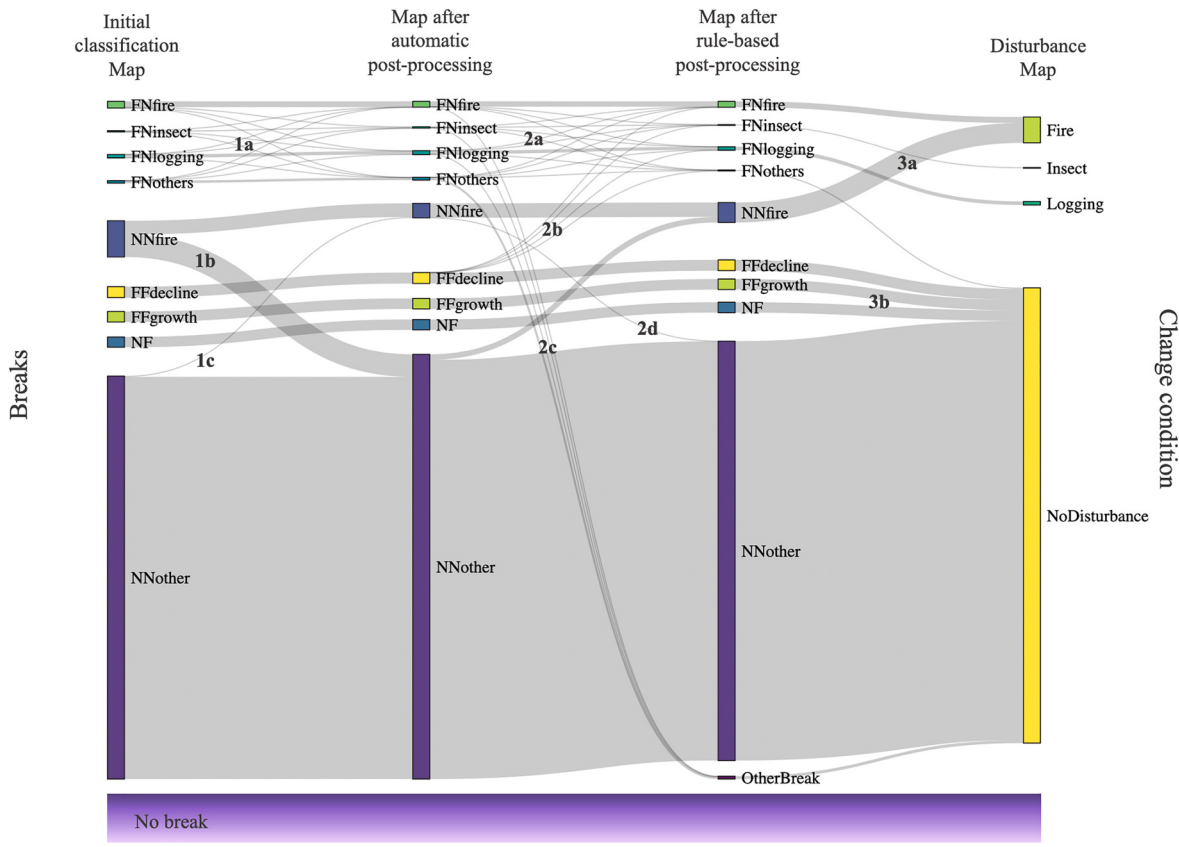


Fig. 4. The sorting of “breaks” into “disturbances” (the Sankey diagram should be read from the left to the right). The first column shows the “breaks” population divided into four major categories (FF, FN, NF, and NN) and classified into multiple disturbance agents (section 2.3). The changes between the first and the second columns are the result of the automatic post-processing (section 2.4). The next step is the rule-based post-processing, which improves the map by optimizing the classification result spatially and temporally within disturbance classes (2a), and taking a small number of samples from FFdecline that have severe condition change to disturbance agents (2b) (section 2.5.2). Disturbances with very low magnitude in column three are removed to other breaks (2c) in column four. FF, NF, NNother, and other breaks are aggregated into the “no disturbance” class (3b), while all FN classes except for FNothers are merged into disturbance agent in the last step (3a).

condition change groups.

The inputs to the classification were the TC BGW indices before the break and Δ TC associated with the breaks. If a pixel has multiple breaks, each break is classified to determine if it is a disturbance, and what kind of disturbance. To serve as training data, 2058 polygons (232,725 pixels) were collected by referencing the synthetic Landsat images, high-resolution imagery on Google Earth, and pest damage perimeters provided by the Canadian Forest Service ([Canadian Council of Forest Ministers, 2019](#)). We also consulted Alberta forest health spatial data from 2005 to 2017 and British Columbia Aerial Overview Survey Data since 1999, including Mountain Pine Beetle heli-GPS data, ariel photography data, spruce budworm and other defoliators' ariel surveys ([\[dataset\] Alberta Agriculture and Forestry, 2018](#); [\[dataset\] The government of British Columbia, 2021](#)). Each sample was assigned to one of the four agents, *fire*, *insect*, *logging*, and *other*, within the years from 1985 to 2014. Though the spectral-temporal signatures of *logging* and *insect* disturbances overlap partially in Δ TC-G, they are well separated in the W and B dimensions (Fig. 5).

2.4. Automated post-processing

To improve the continuity and accuracy of the disturbance maps, we tested multiple post-processing algorithms that included information from auxiliary datasets. We included yearly fire perimeters from the Canadian National Fire Database ([\[dataset\] Canadian Forest Service and Natural Resources Canada, 2019](#)) and the Alaska Fire History Perimeter

Polygons ([\[dataset\] Alaska Wildland Fire Coordinating Group \(AWFCG\) and Alaska Interagency Coordination Center \(AICC\), 2020](#)) in the post-processing. These data sources were used to complement our disturbance map by: (a) cleaning-up the scattered unreliable pixels identified as disturbance; and (b) finding potential unassigned breaks (missed disturbances). Burned agricultural fields were excluded in the disturbance map by applying a cropland mask created from Global Food Security-Support Analysis Data at 30 m ([\[dataset\] Massey et al., 2017](#)).

The intent of the automated post-processing was to remove systematic error by removing scattered, isolated pixels identified as disturbance and smoothing the disturbance types in large patches, where an isolated/scattered pixel is a single disturbance pixel in a 5×5 (pixel) moving window. The CNFD and Alaska historical fire perimeters were merged to create a single fire mask. Moving window operators were designed both spatially and temporally, according to being "in" or "outside" the fire mask. For example, a pixel initially classified as fire disturbance remained classified as fire disturbance when it agreed within a three-year interval fire mask (i.e. the year before, the current year, and the year after). If a pixel classified as fire is "outside" the fire mask, it will be mapped as fire if the plurality of the pixels in a 11×11 (pixel) moving window are fire. Otherwise, it will be changed to the most common disturbance class in the 11×11 (pixel) window. For example, insect and logging pixels were switched to fire if they were "in" the fire perimeters; otherwise, the pixels would change to the plurality class if they were "outside" the fire mask, but in a smaller 5×5 (pixel) moving window.

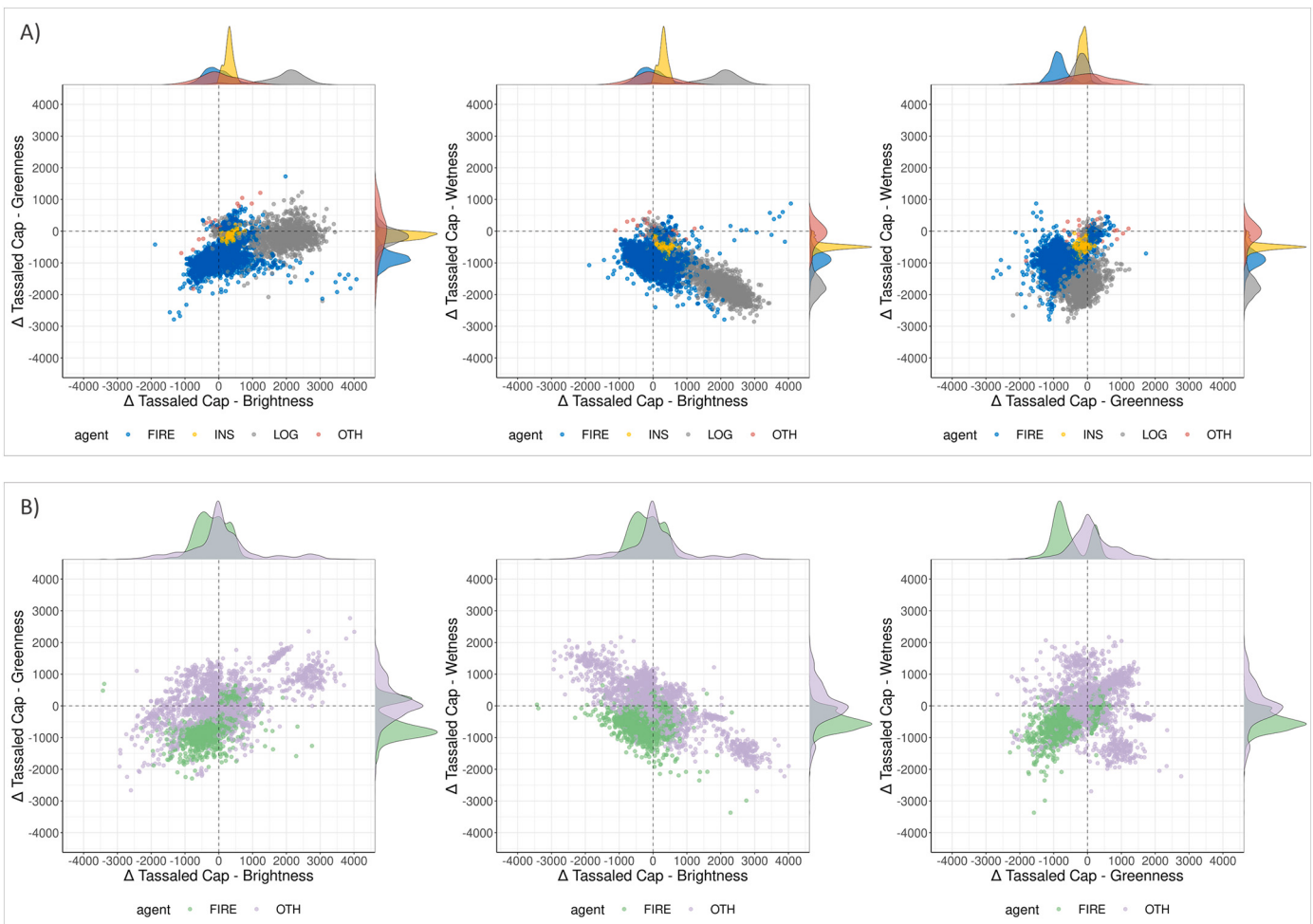


Fig. 5. Training data distribution in Δ TC - brightness, greenness, and wetness planes of A) FN fire (in blue), insect (in yellow), logging (in grey), others (in red) and B) NNfire (in purple) and NNothers (in green) changes. (Δ TC values are shown in units of reflectance $\times 10,000$). (For interpretation of the references to colour in this figure legend, the reader is referred to the web version of this article.)

After applying the automated post-processing, we evaluated a sample of 293 pixels that had changed during the post-processing, and found that more than half had improved as a result of the post-processing (see Supplementary). As the result of the post-processing, approximately 3.56×10^8 of pixels changed classes, or about 5.46% of the breaks detected by CCDC.

2.5. Accuracy assessment and area estimation

Issues that confront all applications of land change monitoring are the accuracy of maps and the uncertainty of area estimates (Olofsson et al., 2014; Stehman and Foody, 2019; Woodcock et al., 2020). In general, to provide reliable land cover and land change information, the “good practice” with regards to sampling design, response design, and analysis can ensure consistent and robust results for assessing accuracy and estimating area of change (Olofsson et al., 2014). Stehman and Foody (2019) pointed out common current problems (i.e., lack of confidence intervals for area estimates, failure to clarify or even use a probability-based sampling design, etc.) and give detailed guidance for specific operational criteria in accuracy assessment. In part, due to improved guidance on accuracy assessment and area estimation, it is now becoming more common for producers of land change information to correct area biases in estimates derived directly from maps by using unbiased estimators applied to reference data collected at locations selected by sampling the study area (Bullock et al., 2018; Curtis et al., 2018; Wickham et al., 2017; Yin et al., 2018). One benefit of these approaches is that they allow quantification of the uncertainty (confidence intervals) for estimates of change.

2.5.1. Reference data and stratification

We collected reference data and performed an accuracy assessment of the maps of disturbance causal agents after the automated post-processing step described in section 2.4. We followed the recommendations in Olofsson et al. (2014) for assessing accuracy and estimating area based on a stratified random sampling. Experience has shown that errors of omission for rare classes (often change classes) that occur in strata with large areas can result in large uncertainties in area estimates (Arévalo et al., 2020b). One strategy for reducing this problem is to minimize the presence of sampling units observed as rare classes in large strata by defining smaller substrata that are more prone to containing omission errors (Olofsson et al., 2020). In our situation, that approach translated into partitioning the “undisturbed” class in our map into multiple, smaller strata in an effort to concentrate any errors of omission for the disturbance classes.

We estimated a total sample size of 1900 units using the stratified variance estimator for n with a target standard error of 0.002 for the insect class (Cochran 1977, Eq. 5.25). The sample units were allocated to strata following the recommendations in Olofsson et al. (2014). The strata and sample allocation were based on a map that combined all the disturbances in the 1987–2012 time period (Table 1). The disturbance strata covered 7.09% of the study area. We divided the remaining “undisturbed” area in the map, which was 92.91% of the study area, into six substrata to avoid the issues associated with omission errors in large strata (Arévalo et al., 2020b). In particular, we tried to identify pixels in the undisturbed stratum that were most likely to include a disturbance. In Table 1, the *NNfire-to-NNother* stratum refers to the pixels that were originally mapped as *NNfire* but changed to *NNother* during the automated post-processing (the “2” stream in Fig. 4). Similarly, *NNother-in-or-near-fire* corresponds to the *NNother* pixels that are in or near the fire pixels in the disturbance map or the fire perimeters from the auxiliary datasets. Our expectation was that our automated post-processing algorithm would occasionally change the class of a pixel when it was correct prior to post-processing. Another stratum was based on pixels we had removed before the Δ TC classification that were *forest* before a break and remained *forest* after a break (according to the map of Wang et al., 2020), but showed a trend of decline (see section 2.3.2 above). We

Table 1

Strata names, description, weight (Wh [%]) based on the stratification map.

| | Strata | Description | W _h | n _h |
|-------------|----------------------|--|----------------|----------------|
| undisturbed | NNfire to NNother | NN pixel changed by post-processing | 3.40 | 100 |
| | NNother in/near fire | NN pixel in the fire perimeter or within 20-pixel buffer | 4.50 | 100 |
| | F- > Fdecline | Forest degradation | 1.63 | 100 |
| | Spatial buffer | 1-pixel spatial buffer of all disturbance pixels | 0.87 | 100 |
| | Other breaks | Model breaks that remain after all others removed | 25.43 | 500 |
| | No break | Stable land covers (no break in the CCDC mode) | 57.08 | 500 |
| disturbed | F- > N fire | Forest loss from fire | 1.49 | 100 |
| | Insect | Forest loss from pest damage | 0.36 | 100 |
| | Logging | Forest loss from harvesting (or associated infrastructure) | 0.77 | 100 |
| | Others | Forest loss from unknown factors | 0.51 | 100 |
| | N- > N fire | Areas of non-forest that burned | 3.95 | 100 |

made these pixels a stratum (*FFdecline*) as they could easily include places where there had been significant insect damage. Also, experience has indicated that pixels near disturbances are more likely to be disturbed than the general population, so we included a “*spatial buffer*” stratum around mapped disturbances (Tyukavina et al., 2013, 2015; Arévalo et al., 2020b). Sometimes one pixel could satisfy multiple strata choices, but the *spatial buffer* was given top priority within the *undisturbed* class. After the pixels that fell in these strata were removed, 25.43% of the pixels remained that had breaks in the CCDC results, and 57.08% that did not have breaks in their CCDC results, and each of these was made a stratum (“*other break*” and “*no break*”). The six strata comprising *undisturbed* were sampled separately, but ultimately combined in the final map and for the process of estimating accuracy and areas.

With the support of Time Series Viewer tool from the Area Estimation & Accuracy Assessment (AREA2) Toolbox (<https://area2.readthedocs.io/>), we visually interpreted 1900 sites from 1987 to 2012, and each sample unit was inspected using Landsat images and Google Earth historical images. Fire and logging can be distinguished from the Landsat images and high-resolution images on Google Earth. Once interpreters recognized a disturbance between 1987 and 2012, they noted the land cover types of the year when the disturbance happened and the year before, and a disturbance agent. The reference data were used to calculate the error matrix, and ultimately the area estimates (Stehman, 2014). Due to the lack of available high-resolution images in the high latitudes and disagreements between the interpreters, we removed 50 ambiguous reference samples and kept 1850 for the analysis.

2.5.2. Lessons learned from the accuracy assessment and subsequent improvement of the maps

The results from the accuracy assessment (see Table. s4) identified several kinds of errors in the disturbance map that we tried to minimize by implementing targeted rules in a second, or “rule-based” round of post-processing. First, *fire* was the most common kind of disturbance being omitted, partially because of the post-processing rules that changed a lot of pixels from *NNfire* to the *NNother* category. This omission error was partially related to the fire perimeters used in the first stage of post-processing, since only fires larger than 200 ha were provided in the fire database. To address this issue, we established an automatic fire detection approach for adding missing fires that were not in the original fire database. After testing numerous thresholds for a spatial moving window size, a new fire mask was generated and added to the existing database. The window size was finally set to 61 × 61 pixels and the disturbance in the window was mapped as fire if the proportion of the fire pixels “outside” the fire database reached an empirical threshold 0.13. Some smaller fires that were missed from both

the fire database and this operation were digitalized manually.

Second, the *FFdecline* stratum was found to include errors of omission, presumably areas that were no longer forest after disturbance. As a result, large-magnitude changes in ΔTC of pixels in the *FFdecline* stratum were classified into one of the causal agents, which depends on the plurality class of surrounding pixels. Third, the three *disturbance* strata had commission errors for mapping *fire*, *insect*, and *logging*, primarily because we expected that all *FN* changes should be disturbances. We removed breaks with extremely low magnitude ΔTC values ($\Delta TC_{B,G,W} < 20$) for this specific case, which corresponds to pathway 2c in Fig. 4. We also modified the moving window size to better separate *insect* from low severity *fire* pixels. Finally, the *FNother* samples proved to be mostly subtle changes, and the only distinct event we found in this class was related to seasonal flooding, causing inundated wetlands to be misclassified as forest and then land cover changes back and forth. Therefore, *FNother* was eliminated from consideration as *disturbance* and merged with the *undisturbed* class. We were careful to define rules without looking at how they would affect the outcome of individual reference observations in the sample. This step was very important, as we used the same reference observations to evaluate the map after the rule-based post-processing, which became the final map.

2.5.3. Estimation of the accuracy of the final map

The rule-based post-processing described in the previous section resulted in changes to the map. As a result, we had reference data that had been stratified using a different map (an initial version) than our final map. When using reference data stratified using one map to assess the accuracy of another map, the traditional stratified estimators are biased, and estimators constructed using indicator functions are required (Stehman, 2014). We constructed estimators following the approach in Stehman, 2014, for estimation of the accuracy of our final map and the areas of the different kinds of disturbance.

2.6. Other products derived from CCDC outputs

In addition to mapping causal agents of disturbance, we also produced a series of products intended to characterize change in landscapes over time. First, we used CCDC to fit harmonic models and predict reflectance values for six bands (Landsat TM and ETM + Bands 1, 2, 3, 4, 5, and 7) for each year, which were used to create gap-free synthetic Landsat images (Zhu et al., 2015). We used the synthetic images in peak summer (Day 212) to help with both training data collection and monitoring changes, and hope other researchers will also benefit from them.

Second, ΔTC images are produced for all model breaks. In addition to disturbances, ΔTC -G and ΔTC -W are indicative of land condition changes such as post-disturbance forest regrowth, forest degradation, and other non-forest related ecological changes relevant to vegetation transitions, changes in surface water, permafrost degradation, response to drought or flooding, and urban expansion (Fig. s1). While we cannot readily or rigorously evaluate the accuracy of these products, we hope they will prove useful to science community who are interested in ecological function and environmental change in arctic and boreal regions.

3. Results

According to the map results, fire dominated the higher latitudes (e.g., Alaska, Yukon Territories, Northwest Territories, and Northern Saskatchewan) in general, while logging activities were mostly found in British Columbia and Alberta in the ABoVE core domain. Pest damage was more scattered and sometimes an outbreak would occur in maps for a few consecutive years. Several major insect outbreaks were found in our maps: one was around Prince George in British Columbia from 2006 to 2010; and the other is near the Great Slave Lake, from 2000 to 2004. We estimated the accuracy of the preliminary map after the automated

post-classification process with the results shown in Section 3.1 and further analyzed the spatial patterns as well as the trends of the disturbed area associated with different agents.

3.1. Accuracy assessment of the map and stratification

Accuracy assessment was performed based on the stratification and map that include changes following the collection of the reference data, or the final map, respectively. The value of the intermediate results based on the stratification was that the sample units in the off-diagonal elements of the confusion matrix (Table s4) were indicative of the issues that drove the need for the rule-based post-processing. The overall accuracy of the intermediate map is $94.7\% \pm 1.18\%$ (all uncertainties are expressed as 95% confidence intervals). However, the user's accuracies of the *fire* and *logging* classes are below 60%, and both user's and producer's accuracy of the *insect* class are below 20%. The rules used in the second round of post-processing were designed to reduce these high rates of omission and commission.

Fire and *logging* were mapped with relatively high user's accuracy ($\geq 95\%$) but had many fire events omitted in non-forest regions, particularly when small in size. The intermediate results of strata comprising *undisturbed* showed that the automated post-processing procedure was too aggressive, as it changed pixels that really were fire to other kinds of disturbance (e.g., *NNfire* to *NNother*). The most common commission errors for *fire* were caused by periodic wetland inundation, drought, and agricultural practices in croplands, which were addressed by rule-based post-processing using land cover maps to differentiate burnt areas from water. Unsurprisingly, the class *insect* had the lowest user's and producer's accuracies, caused by confusion with low severity fire and wrongly sorted into the *FF* category. When viewed on the map, the pixels in the *FFdecline* stratum were surrounded by many disturbance pixels. A few of the sample units from the *FFdecline* stratum were determined to be disturbance and failed to be included in the map, mostly due to errors in the initial land cover maps, and around 2.1% of the *FFdecline* pixels were eventually moved to *disturbance* classes. In the opposite way, errors of commission for the *insect* and *logging* strata were related to low ΔTC magnitudes in the areas defined as *FN* using the original land cover map.

3.2. Post-processing and area estimation of the causal agents

Rule-based post-processing was implemented after becoming aware of the issues identified from the confusion matrix (Table. s4). The overall accuracy of the final map increased to $96.7\% \pm 0.86\%$, and the user's and producer's accuracies for all the disturbance agents improved. The updated fire database not only improved the probability of keeping fire within the perimeters, but also contributed to distinguishing the severe pest damage from low severity fire. Table s1 shows that many of the omitted fire events were corrected by the targeted rules. The adjustment of the window size of the post-processing filters combined with the new fire mask successfully reduced the omission errors in the *NNfire-to-NNother* and *NNother-in-or-near-fire* strata (Table. 2). Additionally, we found the commission errors from the *insect* and *logging* classes decreased after removing pixels with very low magnitude ΔTC values. The last contribution to the improved accuracy is the result of adding the *FF decline* pixels back into consideration for the disturbance class.

Results indicate that 10.8% (with a margin of error of 0.5% at the 95% confidence level) of the ABoVE core domain was disturbed from 1987 to 2012. A total of 39.6% of the disturbance occurred in forested areas. *Fire* was the major disturbance agent and affected $357,101 \text{ km}^2 (\pm 36,437 \text{ km}^2)$, or 8.8% of the study area, over the 26 years. *Logging* ranks second with $55,778 \text{ km}^2 (\pm 17,771 \text{ km}^2)$ of the forest loss, or 1.4% of the ABoVE core domain, during the same time period. Also, a total of $23,786 \text{ km}^2 (\pm 14,283 \text{ km}^2)$ of the forest, or 0.6%, experienced decline and mortality sufficient to merit inclusion in the *insect* class (Fig. 6).

The final map of annual causal agents of disturbance from 1987 to 2012 is shown in Fig. 7. Overall, $291,205 \text{ km}^2$ were mapped as

Table 2

The confusion matrix of the final map (following targeted rule-based post-processing). Numbers in bold are when reference data agree with the map.

| | | Reference | | | |
|--------------------------------------|----------------------|----------------|------------|-----------|---------------|
| | | No Disturbance | Fire | Insect | Logging |
| Map after rule-based post-processing | Other breaks | 748 | 7 | 2 | 5 |
| | NNfire to | 26 | – | – | – |
| | NNother | – | – | – | – |
| | NNother in/near fire | 29 | 7 | – | – |
| | FF decline | 96 | 3 | 4 | 6 |
| | Spatial buffer | 62 | 17 | 1 | 1 |
| | No break | 477 | 1 | 2 | – |
| | Fire | 3 | 246 | – | 1 |
| | Insect | 6 | 5 | 17 | 5 |
| | Logging | 3 | 2 | – | 68 |
| | User's accuracy | 0.967 | 0.980 | 0.633 | 0.885 |
| | Producer's accuracy | 0.997 | 0.777 | 0.222 | 0.546 |
| | Overall accuracy | | | | 96.7% ± 0.86% |

disturbance, and 10% of the forest area in this domain was disturbed by the causes of fire, insect, and/or logging. In Fig. 7, disturbance was upscaled to 900 m for better visualization of the small disturbances. It shows that fire affected large areas in the Northwest Territories (Fig. 7A, region a) before 2000, primarily in non-forest areas. The southern portion of the study domain, like Saskatchewan (in region b of Fig. 7A&B), has a long history of both forest fire and non-forest fire, but the patches tend to be smaller compared to wildfires in Alaska and Yukon. Extensive logging activities occurred in Alberta and British Columbia starting from the early 1990s, usually associated with the roads built a year or two in advance. Salvage logging appeared within the large areas of fire and insect, often found the year after a fire was detected. The areas mapped as logging also include infrastructure developments (e.g. roads, mining). Insect damage is common around the Great Slave Lake between 2001 and 2006, and a severe outbreak was

found from 2004 to 2008 in the Rocky Mountains, which was caused by mountain pine beetles (Fig. 7B) (Coops et al., 2006; Kurz et al., 2008).

On average, disturbance in the ABoVE core domain covers approximately 1700 km² per year since 2000. The mean of the burned area is more than 1436 km² per year; the average logged and insect affected areas are 182 km² and 54 km² per year, respectively. Graphs of the mapped area of disturbance by year reveal that *fire* plays the dominant role across the entire ABoVE study area while *insect* and *logging* are more prominent in Western Canada, mainly because they are more directly related to forest loss (Fig. 8). *Insect* damage and *logging* activities are rare in Alaska when Landsat data are available (after 1999). *Insect* damage has been most extensive since 2000 and reached a peak in 2009. The low rates of disturbance at the end of the analysis in 2011 and 2012 are due to the fact that the CCDC algorithm requires five consecutive observations (during the growing season) to detect a disturbance. Due to the low frequency of clear observations at high latitudes, disturbances later in the study period may be missed. The area of *logging* in Western Canada remains relatively constant at 150–200 km² per year over the entire study period.

3.3. Accuracy assessment of the aggregated disturbance map

Though the map of causal agents provides information on the drivers of disturbance, a simpler and more accurate, aggregated “disturbance” map could be useful. The annual disturbance maps from 1987 to 2012 were assessed using the same reference dataset. The initial strata were collapsed to *disturbance* and *no disturbance*. The overall accuracy of the map was 95.1% ± 0.84%, with all user's and producer's accuracies above or around 90% (Table 3). The estimated area of disturbance in the ABoVE core domain over 26 years was 0.42 million km² (± 39,439 km²), a considerably more precise estimate than the one provided for the individual causes of disturbance (*fire*, *logging*, *insects*).

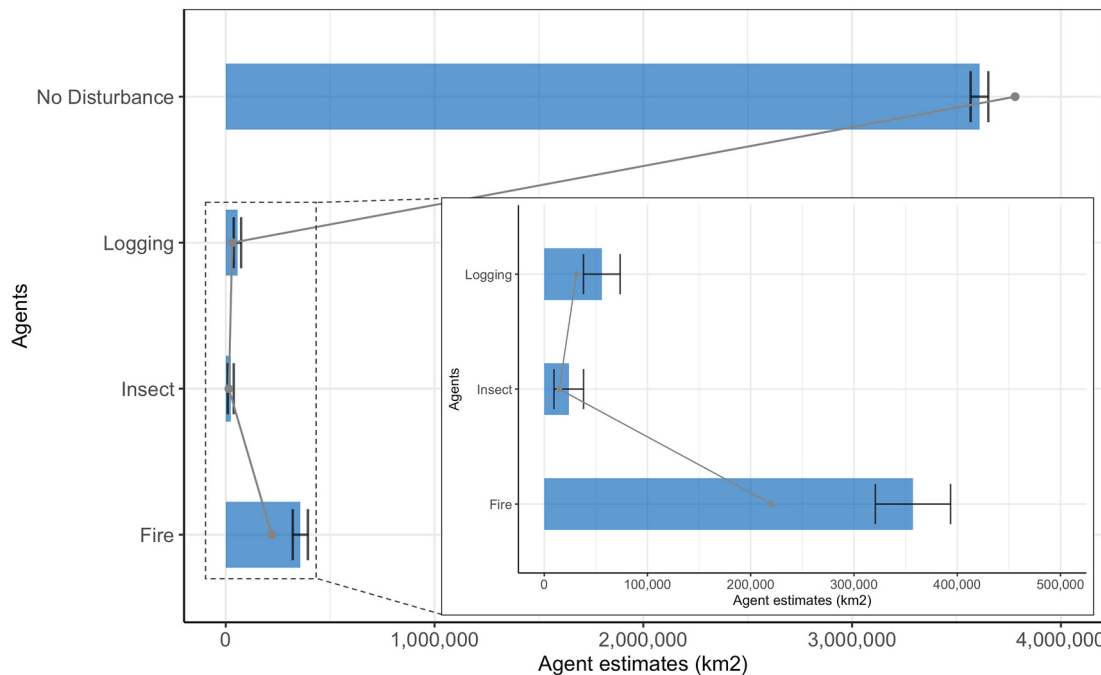


Fig. 6. Area estimates of disturbance agents from 1987 to 2012. Bars in the zoom-in chart are the estimated disturbance area and for comparison purposes, the grey points correspond to the mapped area.

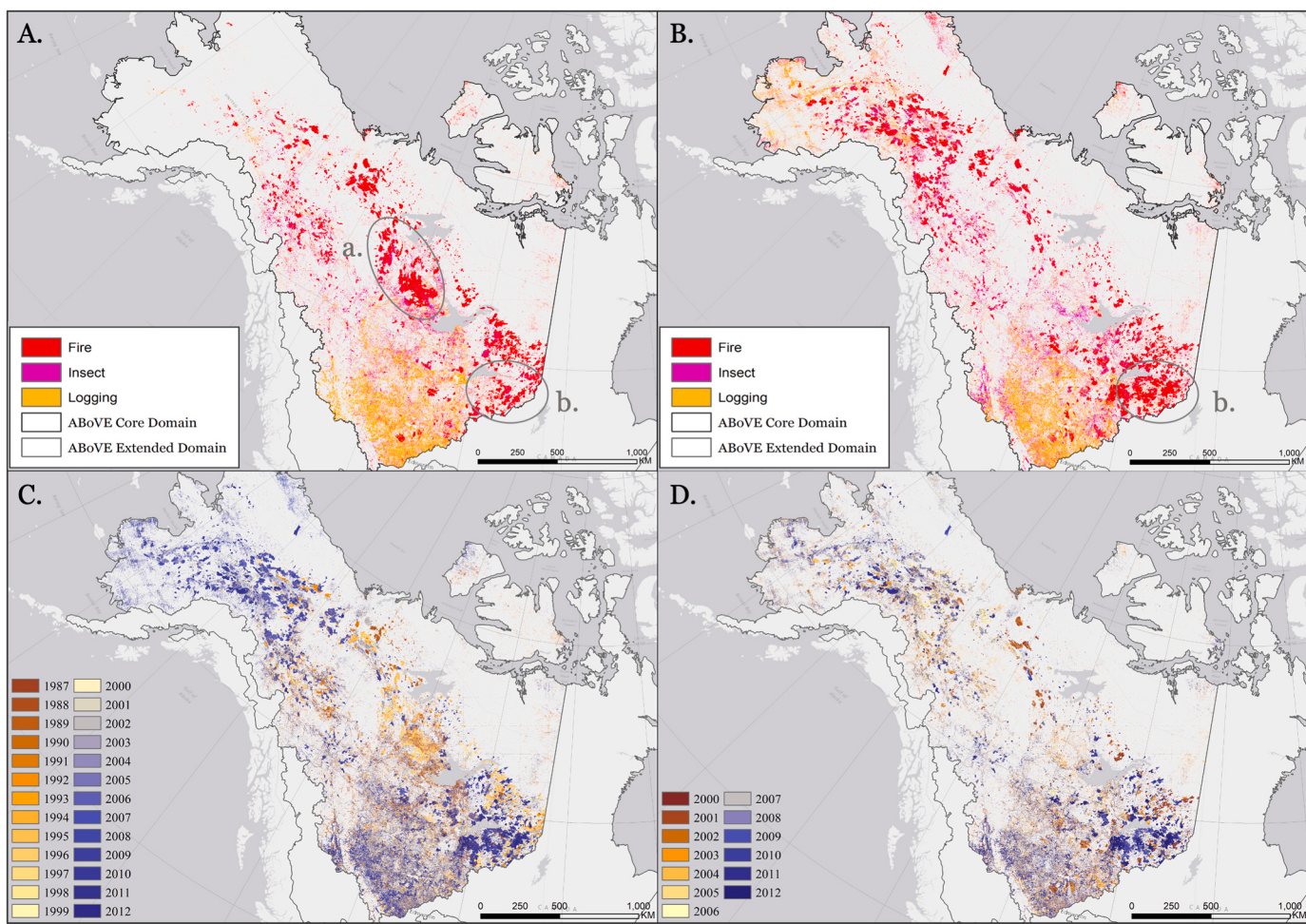


Fig. 7. Disturbance maps upscaled to 900 m resolution with fire, insect, and logging shown. The top two show the most recent disturbance by causal agents for: (A) 1987–1999; and (B) 2000–2012. The bottom two maps are an aggregated “disturbance” map at an annual step in the ABoVE core domain for: (C) 1987–2012; and (D) 2000–2012.

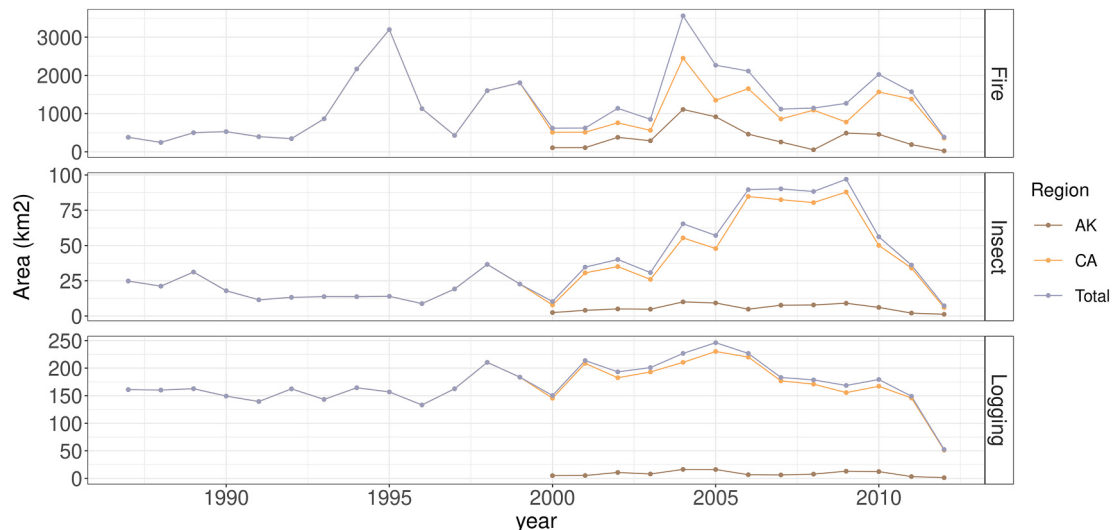


Fig. 8. Mapped areas of three causal agents of disturbance at an annual step (1987–2012). It is important to note that these area estimates are derived from the maps, as we don't have sufficient numbers of reference samples to estimate areas at the annual time scale. For all three kinds of disturbance, the mapped areas are less than the areas estimated using the reference data and the maps. Note that the y-axis for each plot is different. (AK: Alaska; CA: Canada).

Table 3
Confusion matrix of the aggregated disturbance for final map.

| | Reference | No Disturbance | Disturbance |
|--------------------------------------|---------------------|----------------|---------------|
| Map after rule-based post-processing | No Disturbance | 1438 | 62 |
| | Disturbance | 19 | 331 |
| | User's accuracy | 0.959 | 0.946 |
| | Producer's accuracy | 0.980 | 0.893 |
| | Overall accuracy | | 95.1% ± 0.84% |

4. Discussion

4.1. Mapping the causal agents

In this paper, we mapped causal agents of disturbance annually in the ABoVE core domain at an annual step at 30 m using Landsat time-series data from 1984 to 2014. We attributed the causes of disturbance to fire, insect, and logging, and categorized the land condition change by differentiating it from disturbances. The ancillary data, particularly fire perimeters and insect inventory data, made a significant contribution to the post-processing procedure, while at the same time, our results indicate we found missing fires that current products have not included.

Table 4 shows that there are 22,506 km² of fire in our results that are outside the perimeters of the existing database. In some respects that is not surprising, as the existing database don't include fire less than 2 km² in size. Because the producer's accuracy of our fire results is quite high (98%, or 2% omission rate), it is likely these areas really are fires. If anything, there may be an underestimate of the extent of fire outside existing databases as more errors of omission than commission for fire were found in our results. For investigators interested in the location and extent of fires, there has very useful information in our maps.

Additionally, it is interesting to note that there is a substantial area inside the perimeters of the fires in the existing databases that did not burn (Fig. 9). Table 4 shows that according to our maps, 125,254 km² out of a total 385,573 km² within the fire perimeters was not burned. Since the existing databases are, in fact, perimeters, and not maps of the extent of burned area, this result is not surprising. Hopefully our results shed some light on the proportion of the area within the perimeters that remains unburned (32%; roughly one third). Fig. 9 shows an example of the differences between our results and the fire databases. The results of a comparison of our reference samples with the existing fire databases show similar trends in terms of missed fires in the databases and unburned areas within fire perimeters. It is hard to translate the data in Table. s6 into area estimates, as the samples in the reference dataset are from a stratified sample, and they carry different inclusion probabilities. But it is reassuring that they show the same basic patterns as the comparison with our maps.

Before 2000, as Fig. 8 shows, the average burned area per year was 1045.3 km², and peaked in 1995 at three times the average. The years 1994, 1998, and 1999 also had very large burned areas. The years with the largest fires corresponded to the 1990–1995 recorded El Niño (EN) events, which had a drier climate and eventually brought drought-

induced fire (Trenberth and Hoar, 1996). After 2000, the trends of fire are almost the same in Alaska and Western Canada, with the yearly burned area 60 km² higher than pre- 2000. Big fires occurred in 2004–2006 and 2010, and logging remained at a higher rate between 1998 and 2006. Pest damage accounts for 19 km² before 2000 in the Provinces of Western Canada, but increased by a factor of three to 52 km² per in the years since 2000 and continued increasing until 2009.

The enlarged image chips in Fig. 10 show two examples of the yearly disturbances. Fig. 10-A shows accumulated disturbance caused by multiple drivers in British Columbia, Canada, for 26 years. This region experienced multiple kinds of disturbance, including harvesting, fire, mountain pine beetle damage followed by salvage logging. Comparison of the synthetic images in 1986 and 2012 shows that over two-thirds of this area experienced disturbance and 87.6% of the forest was lost by the end of 2012. The other example (Fig. 10-B) shows the cumulative forest harvesting from 1987 to 2012 and the associated agricultural expansion, where the disturbance maps overlaid on synthetic images from the starting and ending years show that most of the land transitions in this area are caused by human activities.

The Kenai Peninsula is the most northern place where we found insect damage in our maps. Since the disturbance map was processed based on the ABoVE Reference Grid (Loboda et al., 2019), some disturbances in the ABoVE extended domain were not displayed in Fig. 7. Fig. 11 shows the effect of spruce beetles in the Kenai Peninsula from 1990 to 2004, which became apparent after Landsat data began being collected in Alaska after 1999, and this outbreak continued for several years. There is a long history of regional beetle outbreaks among spruce forests starting in the late 1980s on the Kenai Peninsula (Berg et al., 2006; Jones, 2008). Our results indicate annual insect-induced disturbance of about 4.5 km² within the region shown in Fig. 11. Our results also show that the pest damage in this region from 2005 to 2010 dropped by 90% compared to 1999–2004.

4.2. Advantages of using ΔTC and remained challenges

Based on the detection of land cover and land condition changes using CCDC, this study develops a new approach using ΔTC indices for sorting “breaks” into causes of disturbance. The advantage of using multi-dimension ΔTC indices is that the principal information from all the original Landsat bands is included, which improves performance relative to a single Landsat spectral band or a single index. For example, while it is common for deciduous forests to decrease in both wetness and greenness after a disturbance, conifer forests will often increase in greenness. This asynchronous response indicates the loss of forest or “browning” may not be caused by drought, since increases in wetness can also lead to a less “green” spectral signal. Similarly, more precipitation and groundwater do not always result in greening. Therefore, multidimensional indices are helpful for characterizing the changes in coniferous forests and boreal biomes.

The most challenging part of mapping the causal agents is the similar spectral-temporal signals of the change for insect damage and low severity fire, or the edges of fire. By implementing rule-based post-processing and developing more reliable fire perimeters, we attempted to reduce this confusion. The results demonstrate a feasible framework of mapping the insect damage along with other causes of disturbance using the Landsat time series. However, the high omission error (low producer accuracy) for the insect disturbance (Table. 2) can be attributed to multiple reasons and requires further improvement. First, although ΔTC indices were helpful for differentiating causal agents, tracking subtle and gradual changes relies on the ability of “break” detection by the CCDC model. A possible way to improve the accuracy of gradual change is to identify the transitional segments with significant slope for the model fits and classify these segments. However, the remaining challenge will be to distinguish the spectral differences between insect and drought. Secondly, as the designed sub-stratum “FFdecline” indicated, the forest could be attacked by different kinds of

Table 4

Comparison between ancillary fire database against the mapped fire in our disturbance map. The burned area was counted from 1987 to 2012 in Western Canada and 2000 to 2020 for Alaska (unit: km²).

| | Fire database | |
|-------------------------|---------------|-----------|
| | Fire | Not Fire |
| Fire in disturbance map | 260,319 | 22,506 |
| Not fire | 125,254 | 4,905,521 |

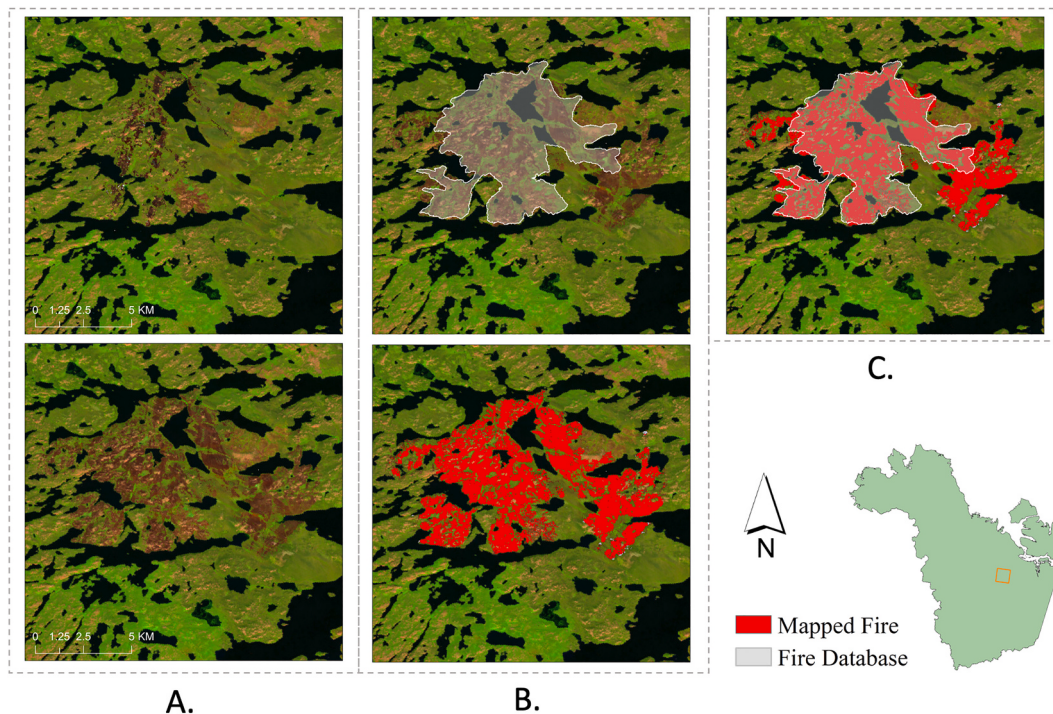


Fig. 9. Comparison between the fire database and the disturbance map of a fire event in Northwest Territory in 2005. Column A is synthetic images in SWIR1, NIR, Red (stretched to 0 to 4000) bands in 2005 (upper) and 2006 (bottom). The land cover type is mostly wetlands with shrub and herbaceous vegetation, and the black areas are water. The upper figure in column B is the fire database from year 2005 overlaid on the 2006 synthetic image; the bottom figure is the mapped fire disturbance overlaid on the 2006 synthetic image. Column C is the overlay of the fire database and mapped fire on the 2006 synthetic image. Note that not all areas with the fire perimeter burned, and some of the fire spread outside the fire perimeter. (For interpretation of the references to colour in this figure legend, the reader is referred to the web version of this article.)

insect (e.g. defoliators v.s. bark beetles), so the spectra will behave differently depending on the condition of the trees. This issue requires more training samples for pest damage that do not cause forest loss. Third, since insect disturbances are not as extensive and frequent as fire, a few omitted insect samples can cause low producer's accuracy as *insect* is relatively a rare stratum. Another potential way to improve the insect mapping is adding spatial information during the classification or post-processing step, considering the spatially diffuse patterns of certain types of insect outbreaks.

Another difficulty was to differentiate *fire* in non-forest regions from periodically inundated wetlands. One way to improve the map in future work may be to include the thermal band, which should increase the accuracy of mapping *fire* by excluding wetlands change.

In addition to forming the basis of the disturbance map, ΔTC images also provide information on changes in land condition, particularly changes in greenness (ΔTC-G) and wetness (ΔTC-W). For example, the ΔTC indices reveal changes in greenness and wetness in the tundra region at an annual time step, and these patterns can be used to study the dynamics of arctic and boreal ecosystems and how they relate to climate variability.

4.3. Lessons learned from reference data collection

We employed a slightly different approach to the use of reference data than most past studies. It is now common practice in studies of environmental change to use a map to stratify the study area in a design-based approach for accuracy assessment and area estimation. The reference data are rarely used to improve the map even though the pattern and magnitude of classification errors are identified. In this study, we used the information obtained when comparing the reference data and the map to improve the underlying map. When we were developing the methods for improving the map, we were careful not to

refer back to the reference data or "tune" the results based on the reference data. As a result, the sample data could still be used but required a more complex analysis based on estimators constructed using indicator functions (Stehman, 2014). We found this approach helpful and it improved our final result. We expect approaches like this to become more common.

It is important to note that estimates of the area of classes that include both the reference data and the map will differ from those based just on the map. For example, the map shows that 7.2% of the study area was disturbed between 1987 and 2012, which is an underestimate given the results reported above.

5. Conclusion

Approximately $2.9 \times 10^5 \text{ km}^2$ of the ABoVE core domain experienced disturbance from 1984 to 2014. Fire was the dominant cause of forest loss and other land cover transitions, while insect damage for this region was prominently observed from 2000 to 2009. Insect damage was found in Kenai Peninsula and Yukon Territories in our annual maps, much farther north than the better documented main areas of insect damage in British Columbia and Northwest Territories. We utilized CCDC, which uses Landsat time series for change detection. We found that ΔTC indices help identify the different causal agents of *fire*, *insect*, and *logging* in the arctic-boreal domain. To differentiate multiple causes of disturbance with similar magnitudes, an automated post-processing step improved our results. Dividing the undisturbed areas in our map into multiple strata provided an opportunity to target specific problems identified by our reference dataset with a rule-based post-processing step that improved our final results. The final disturbance maps have improved fire characterization, including many small fires that are not in other fire perimeter products.

Future efforts will focus on extending the products in time and space

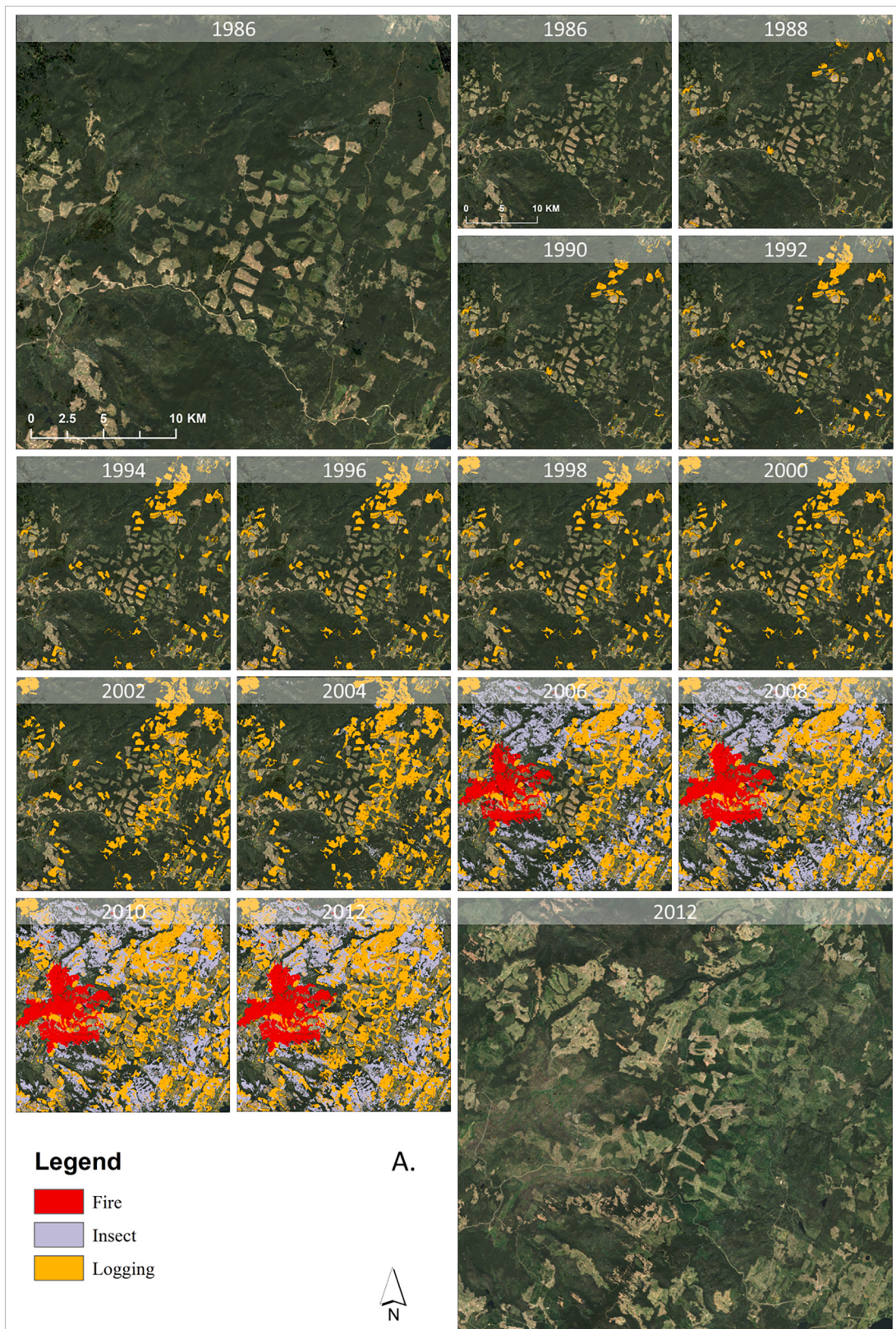


Fig. 10. Two sites that experienced extensive disturbance in the 26 years of this study. The first and the last image chips of both sites are the synthetic images (shown in Red, Green, and Blue band, stretched from 0 to 1500) of 1986 and 2012, respectively. Between those years, annual maps show the accumulated disturbances overlaid on synthetic images. (For interpretation of the references to colour in this figure legend, the reader is referred to the web version of this article.)

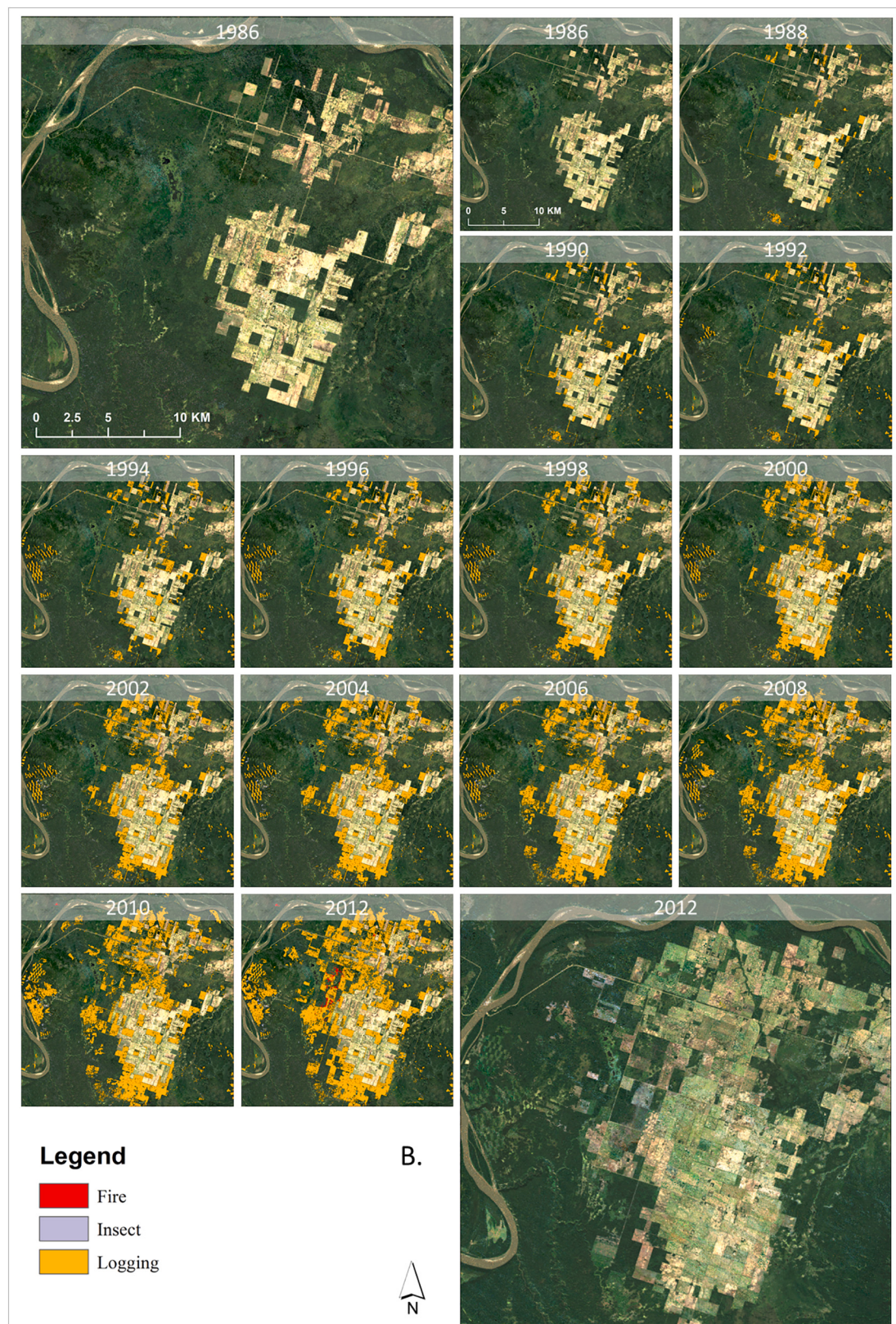


Fig. 10. (continued).

and explore integration of other satellite data (e.g., Sentinel 2 and Harmonized Landsat Sentinel-2 (HLS)). Another potential way to improve the result will be training the classifiers separately for each eco-zone, as there are spectral-temporal differences for various kinds of

insects and tree species across the entire domain. In addition to mapping disturbance, changes in vegetation condition at annual time steps can be used to understand patterns of the greening and browning in arctic ecosystems.

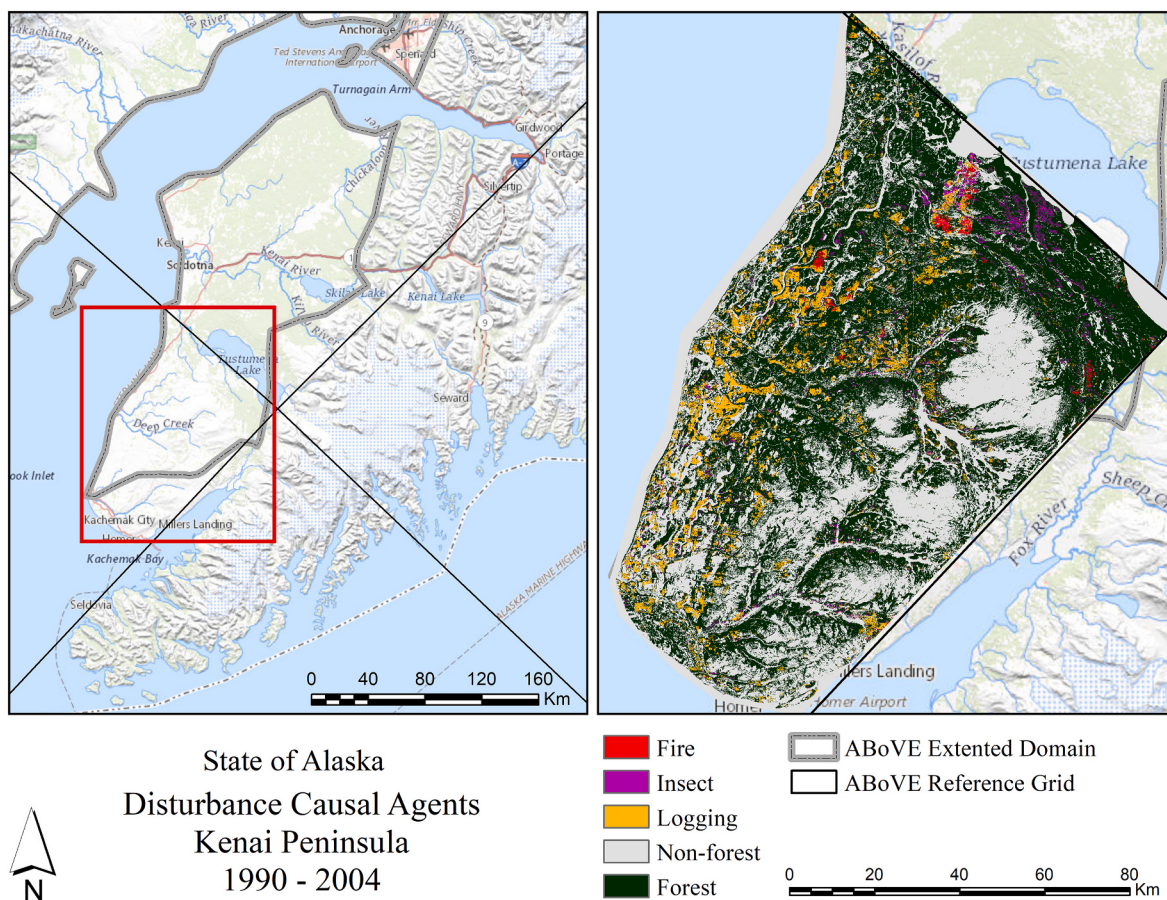


Fig. 11. Multiple disturbances affected the Kenai Peninsula from 1990 to 2004. Pest damage was observed during this period, mainly near Tustumena Lake. (There aren't Landsat observations in this area from 1992 to 1998).

CRediT authorship contribution statement

Yingtong Zhang: Conceptualization, Methodology, Data curation, Formal analysis, Software, Investigation, Visualization, Validation, Writing – original draft, Writing – review & editing. **Curtis E. Woodcock:** Conceptualization, Methodology, Supervision, Writing – review & editing, Project administration, Funding acquisition. **Shijuan Chen:** Formal analysis, Writing – review & editing. **Jonathan A. Wang:** Data curation, Writing – review & editing. **Damien Sulla-Menashe:** Data curation, Software, Writing – review & editing. **Zhenpeng Zuo:** Validation, Writing – review & editing. **Pontus Olofsson:** Investigation, Validation, Writing – review & editing. **Yetianjian Wang:** Formal analysis. **Mark A. Friedl:** Writing – review & editing, Project administration, Funding acquisition.

Declaration of Competing Interest

The authors declare that they have no known competing financial interests or personal relationships that could have appeared to influence the work reported in this paper.

Acknowledgements

This work was supported by the NASA ABoVE [grant number NNX15AU63A], Landsat Science Team funding [grant number 140G118C0006], and NASA MEaSUREs [grant number 80NSSC18K0994]. The author would like to thank Yaxiong Ma, Xiaojing Tang, Paulo Arévalo, and Eric Bullock for the help and general discussions; Tian Li, Katelyn Tarrio, Keila Munz, Keming Bu, Xinyuan Li, Chen

Tang for helping with training/reference data collection; Chris Holden for pre-processing the Landsat data. The authors would also like to thank the associate editor and three anonymous reviewers, whose insightful comments and suggestions helped improve this manuscript.

Appendix A. Supplementary data

Supplementary data to this article can be found online at <https://doi.org/10.1016/j.rse.2022.112935>.

References

- Alaska Wildland Fire Coordinating Group (AWFCG) and Alaska Interagency Coordination Center (AICC), 2020. Alaska Fire History Perimeter Polygons. <https://fire.ak.blm.gov/predsvcs/maps.php>.
- Alberta Agriculture and Forestry, 2018. Forest Health Spatial Data. <https://www.alberta.ca/forestry.aspx?cat1=Mountain%20Pine%20Beetle%20in%20Alberta&cat2=Alberta%27s%20Strategy&cat3=MPB%20Mortality%20Survey%20Results>.
- Alcaraz-Segura, D., Chuvieco, E., Epstein, H.E., Kasischke, E.S., Trishchenko, A., 2010. Debating the greening vs. browning of the north American boreal forest: differences between satellite datasets. *Glob. Chang. Biol.* 16, 760–770. <https://doi.org/10.1111/j.1365-2486.2009.01956.x>.
- Arévalo, P., Bullock, E.L., Woodcock, C.E., Olofsson, P., 2020a. A suite of tools for continuous land change monitoring in google earth engine. *Front. Clim.* 2, 576740. <https://doi.org/10.3389/fclim.2020.576740>.
- Arévalo, P., Olofsson, P., Woodcock, C.E., 2020b. Continuous monitoring of land change activities and post-disturbance dynamics from Landsat time series: a test methodology for REDD+ reporting. *Remote Sens. Environ.* 238, 111051 <https://doi.org/10.1016/j.rse.2019.01.013>.
- Berg, E.E., David Henry, J., Fastie, C.L., De Volder, A.D., Matsuoka, S.M., 2006. Spruce beetle outbreaks on the Kenai Peninsula, Alaska, and Kluane National Park and Reserve, Yukon Territory: relationship to summer temperatures and regional differences in disturbance regimes. *For. Ecol. Manag.* 227, 219–232. <https://doi.org/10.1016/j.foreco.2006.02.038>.

- Bhatt, U.S., Walker, D.A., Reynolds, M.K., Comiso, J.C., Epstein, H.E., Jia, G., Gens, R., Pinzon, J.E., Tucker, C.J., Tweedie, C.E., 2010. Circumpolar Arctic tundra vegetation change is linked to sea ice decline. *Earth Interat.* 14, 1–20.
- Bonan, G.B., 2008. Forests and climate change: forcings, feedbacks, and the climate benefits of forests. *Science* 30 (320), 1444 LP – 1449.
- Bond-Lamberty, B., Peckham, S.D., Ahl, D.E., Gower, S.T., 2007. Fire as the dominant driver of Central Canadian boreal forest carbon balance. *Nature* 450, 89–92. <https://doi.org/10.1038/nature06272>.
- Breiman, L., 2001. Random forests. *Mach. Learn.* 45, 5–32. <https://doi.org/10.1023/A:1010933404324>.
- Bright, B.C., Hudak, A.T., Meddens, A.J.H., Egan, J.M., Jorgensen, C.L., 2020. Mapping multiple insect outbreaks across large regions annually using landsat time series data. *Remote Sens.* 12, 1655. <https://doi.org/10.3390/rs12101655>.
- Bullock, E.L., Woodcock, C.E., Olofsson, P., 2018. Monitoring tropical forest degradation using spectral unmixing and Landsat time series analysis. *Remote Sens. Environ.* 110968 <https://doi.org/10.1016/J.RSE.2018.11.011>.
- Burton, P.J., Boulanger, Y., 2018. Characterizing combined fire and insect outbreak disturbance regimes in British Columbia, Canada. *Landsc. Ecol.* 33, 1997–2011. <https://doi.org/10.1007/s10980-018-0710-4>.
- Canadian Council of Forest Ministers, 2019. National Forestry Database - Canada (Version 2.0.0) [Data set]. Zenodo. <https://doi.org/10.5281/zenodo.3843429>.
- Canadian Forest Service, Natural Resources Canada, Canadian Forest Service, Northern Forestry Centre, Edmonton, Alberta, 2019. Canadian National Fire Database – Agency Fire Data. <https://cwfis.cfs.nrcan.gc.ca/datamart/metadata/nfdbpt>.
- Chapin, F.S., Sturm, M., Serreze, M.C., McFadden, J.P., Key, J.R., Lloyd, A.H., McGuire, A.D., Rupp, T.S., Lynch, A.H., Schimel, J.P., Beringer, J., Chapman, W.L., Epstein, H.E., Euskirchen, E.S., Hinzman, L.D., Jia, G., Ping, C.-L., Tape, K.D., Thompson, C.D.C., Walker, D.A., Welker, J.M., 2005. Role of land-surface changes in arctic summer warming. *Science* 30 (310). <https://doi.org/10.1126/science.1117368>, 657 LP – 660.
- Cohen, W.B., Spies, T.A., Fiorella, M., 1995. Estimating the age and structure of forests in a multi-ownership landscape of western Oregon, U.S.A. *Int. J. Remote Sens.* 16, 721–746. <https://doi.org/10.1080/01431169508954436>.
- Cohen, W.B., Yang, Z., Healey, S.P., Kennedy, R.E., Gorelick, N., 2018. A LandTrendr multispectral ensemble for forest disturbance detection. *Remote Sens. Environ.* 205, 131–140. <https://doi.org/10.1016/j.rse.2017.11.015>.
- Collins, J.B., Woodcock, C.E., 1996. An assessment of several linear change detection techniques for mapping forest mortality using multitemporal landsat TM data. *Remote Sens. Environ.* 56, 66–77. [https://doi.org/10.1016/0034-4257\(95\)00233-2](https://doi.org/10.1016/0034-4257(95)00233-2).
- Coops, N.C., Wulder, M.A., White, J.C., 2006. Integrating remotely sensed and ancillary data sources to characterize a mountain pine beetle infestation. *Remote Sens. Environ.* 105, 83–97. <https://doi.org/10.1016/J.RSE.2006.06.007>.
- Coops, N.C., Shang, C., Wulder, M.A., White, J.C., Hermosilla, T., 2020. Change in forest condition: characterizing non-stand replacing disturbances using time series satellite imagery. *For. Ecol. Manag.* 474, 118370 <https://doi.org/10.1016/j.foreco.2020.118370>.
- Crist, E.P., Cicone, R.C., 1984. A physically-based transformation of thematic mapper data—the TM tasseled cap. *IEEE Trans. Geosci. Remote Sens.* GE-22, 256–263. <https://doi.org/10.1109/TGRS.1984.350619>.
- Curtis, P.G., Slay, C.M., Harris, N.L., Tyukavina, A., Hansen, M.C., 2018. Classifying drivers of global forest loss. *Science* 361, 1108–1111. <https://doi.org/10.1126/science.aau3445>.
- de Wit, H.A., Bryn, A., Hofgaard, A., Karstensen, J., Kvælevåg, M.M., Peters, G.P., 2014. Climate warming feedback from mountain birch forest expansion: reduced albedo dominates carbon uptake. *Glob. Chang. Biol.* 20, 2344–2355. <https://doi.org/10.1111/gcb.12483>.
- Esprito-Santo, F.D.B., Gloor, M., Keller, M., Malhi, Y., Saatchi, S., Nelson, B., Junior, R.C. O., Pereira, C., Lloyd, J., Frolking, S., Palace, M., Shimabukuro, Y.E., Duarte, V., Mendoza, A.M., López-González, G., Baker, T.R., Feldpausch, T.R., Brienen, R.J.W., Asner, G.P., Boyd, D.S., Phillips, O.L., 2014. Size and frequency of natural forest disturbances and the Amazon forest carbon balance. *Nat. Commun.* 5, 1–6. <https://doi.org/10.1038/ncomms4434>.
- Fisher, J.B., Hayes, D.J., Schwalm, C.R., Huntzinger, D.N., Stofferahn, E., Schaefer, K., Luo, Y., Wullschleger, S.D., Goetz, S., Miller, C.E., 2018. Missing pieces to modeling the Arctic-Boreal puzzle. *Environ. Res. Lett.* 13, 2020.
- Franklin, S., Robitaille, S., 2020. Forest insect defoliation and mortality classification using annual Landsat time series composites: a case study in northwestern Ontario, Canada. *Remote Sens. Lett.* 11, 1175–1180. <https://doi.org/10.1080/2150704X.2020.1828659>.
- Frazier, R.J., Coops, N.C., Wulder, M.A., 2015. Boreal shield forest disturbance and recovery trends using Landsat time series. *Remote Sens. Environ.* 170 <https://doi.org/10.1016/j.rse.2015.09.015>.
- Frazier, R.J., Coops, N.C., Wulder, M.A., Hermosilla, T., White, J.C., 2018. Analyzing spatial and temporal variability in short-term rates of post-fire vegetation return from Landsat time series. *Remote Sens. Environ.* 205, 32–45. <https://doi.org/10.1016/j.rse.2017.11.007>.
- French, N.H.F., Kasischke, E.S., Hall, R.J., Murphy, K.A., Verbyla, D.L., Hoy, E.E., Allen, J.L., 2008. Using Landsat data to assess fire and burn severity in the North American boreal forest region: an overview and summary of results. *Int. J. Wildland Fire* 17, 443–462. <https://doi.org/10.1071/WF08007>.
- Gao, B.C., 1996. NDWI—A normalized difference water index for remote sensing of vegetation liquid water from space. *Remote Sens. Environ.* 58, 257–266. [https://doi.org/10.1016/S0034-4257\(96\)00067-3](https://doi.org/10.1016/S0034-4257(96)00067-3).
- Healey, S.P., Cohen, W.B., Zhiqiang, Y., Krankina, O.N., 2005. Comparison of Tasseled Cap-based Landsat data structures for use in forest disturbance detection. *Remote Sens. Environ.* 97, 301–310. <https://doi.org/10.1016/j.rse.2005.05.009>.
- Hermosilla, T., Wulder, M.A., White, J.C., Coops, N.C., Hobart, G.W., Campbell, L.B., 2016. Mass data processing of time series Landsat imagery: pixels to data products for forest monitoring. *Int. J. Digit. Earth* 9, 1035–1054. <https://doi.org/10.1080/17538947.2016.1187673>.
- Hermosilla, T., Wulder, M.A., White, J.C., Coops, N.C., 2019. Prevalence of multiple forest disturbances and impact on vegetation regrowth from interannual Landsat time series (1985–2015). *Remote Sens. Environ.* 233, 111403 <https://doi.org/10.1016/j.rse.2019.111403>.
- Hlášny, T., König, L., Krokene, P., Lindner, M., Montagné-Huck, C., Müller, J., Qin, H., Raffa, K.F., Schelhaas, M.J., Svoboda, M., Viiri, H., Seidl, R., 2021. Bark beetle outbreaks in Europe: state of knowledge and ways forward for management. *Curr. For. Rep.* <https://doi.org/10.1007/s40725-021-00142-x>.
- Holden, C.E., 2017. Yet Another Time Series Model (YATSM). Zenodo. <https://doi.org/10.5281/zenodo.17129>.
- Huang, C., Goward, S.N., Masek, J.G., Thomas, N., Zhu, Z., Vogelmann, J.E., 2010. An automated approach for reconstructing recent forest disturbance history using dense Landsat time series stacks. *Remote Sens. Environ.* 114, 183–198. <https://doi.org/10.1016/j.rse.2009.08.017>.
- Hugelius, G., Strauss, J., Zubrzycki, S., Harden, J.W., Schuur, E.A.G., Ping, C.L., Schirmeister, L., Grosje, G., Michaelson, G.J., Koven, C.D., O'Donnell, J.A., Elberling, B., Mishra, U., Camill, P., Yu, Z., Palmtag, J., Kuhry, P., 2014. Estimated stocks of circumpolar permafrost carbon with quantified uncertainty ranges and identified data gaps. *Biogeosciences* 11, 6573–6593. <https://doi.org/10.5194/bg-11-6573-2014>.
- Johnstone, J.F., Hollingsworth, T.N., Chapin, F.S., Mack, M.C., 2010. Changes in fire regime break the legacy lock on successional trajectories in Alaskan boreal forest. *Glob. Chang. Biol.* 16, 1281–1295. <https://doi.org/10.1111/j.1365-2486.2009.02051.x>.
- Jones, B.M., 2008. *The Face of Alaska: A Look at Land Cover and the Potential Drivers of Change* (No. 2008–1161). Geological Survey (US).
- Ju, J., Masek, J.G., 2016. The vegetation greenness trend in Canada and US Alaska from 1984–2012 Landsat data. *Remote Sens. Environ.* 176, 1–16. <https://doi.org/10.1016/j.rse.2016.01.001>.
- Ju, J., Roy, D.P., 2008. The availability of cloud-free Landsat ETM+ data over the conterminous United States and globally. *Remote Sens. Environ.* 112, 1196–1211. <https://doi.org/10.1016/J.RSE.2007.08.011>.
- Kasischke, E.S., Goetz, S.J., Kimball, J.S., Mack, M.C., 2010a. *The Arctic-Boreal Vulnerability Experiment (ABOVE): A Concise Plan for a NASA-Sponsored Field Campaign* (Final report on the VuRSAL/ABOVE scoping Study).
- Kasischke, Eric S., Verbyla, D.L., Rupp, T.S., McGuire, A.D., Murphy, K.A., Jandt, R., Barnes, J.L., Hoy, E.E., Duffy, P.A., Calef, M., Turetsky, M.R., 2010b. Alaska's changing fire regime - implications for the vulnerability of its boreal forests. *Can. J. For. Res.* 40, 1313–1324. <https://doi.org/10.1139/X10-098>.
- Kennedy, R.E., Yang, Z., Cohen, W.B., 2010. Detecting trends in forest disturbance and recovery using yearly Landsat time series: 1. LandTrendr - temporal segmentation algorithms. *Remote Sens. Environ.* 114, 2897–2910. <https://doi.org/10.1016/j.rse.2010.07.008>.
- Kennedy, R.E., Yang, Z., Gorelick, N., Braaten, J., Cavalcante, L., Cohen, W.B., Healey, S., 2018. Implementation of the LandTrendr algorithm on google earth engine. *Remote Sens.* <https://doi.org/10.3390/rs10050691>.
- Key, C.H., Benson, N.C., 2003. The normalized burn ratio (NBR): A Landsat TM radiometric measure of burn severity. In: US Geological Survey Northern Rocky Mountain Science Center. U.S. Department of the Interior, U.S. Geological Survey, Northern Rocky Mountain Science Center.
- Kurz, W.A., Dymond, C.C., Stinson, G., Rampey, G.J., Neilson, E.T., Carroll, A.L., Ebata, T., Safranyik, L., 2008. Mountain pine beetle and forest carbon feedback to climate change. *Nature* 452, 987.
- Lawrence, P.J., Chase, T.N., 2010. Investigating the climate impacts of global land cover change in the community climate system model. *Int. J. Climatol.* 30, 2066–2087. <https://doi.org/10.1002/joc.2061>.
- Li, M., Huang, C., Zhu, Z., Shi, H., Lu, H., Peng, S., 2009a. Assessing rates of forest change and fragmentation in Alabama, USA, using the vegetation change tracker model. *For. Ecol. Manag.* 257, 1480–1488. <https://doi.org/10.1016/j.foreco.2008.12.023>.
- Li, M., Huang, C., Zhu, Z., Wen, W., Xu, D., Liu, A., 2009b. Use of remote sensing coupled with a vegetation change tracker model to assess rates of forest change and fragmentation in Mississippi, USA. *Int. J. Remote Sens.* 30, 6559–6574. <https://doi.org/10.1080/01431160903241999>.
- Liaw, A., Wiener, M., 2002. Classification and regression by randomForest. *R News* 2 (3), 18–22.
- Loboda, T.V., Chen, D., Hall, J.V., He, J., 2018. ABove: Landsat-derived Burn Scar dnBr across Alaska and Canada, 1985–2015. ORNL DAAC, Oak Ridge, Tennessee, USA. <https://doi.org/10.3334/ORNLDAAC/1564>.
- Loboda, T.V., Hoy, E.E., Carroll, M.L., 2019. ABove: Study Domain and Standard Reference Grids, Version 2. ORNL DAAC, Oak Ridge, Tennessee, USA. <https://doi.org/10.3334/ORNLDAAC/1527>.
- Loveland, T.R., Dwyer, J.L., 2012. Landsat: building a strong future. *Remote Sens. Environ.* 122, 22–29. <https://doi.org/10.1016/j.rse.2011.09.022>.
- Masek, J.G., Huang, C., Wolfe, R., Cohen, W., Hall, F., Kutler, J., Nelson, P., 2008. North American forest disturbance mapped from a decadal Landsat record. *Remote Sens. Environ.* 112, 2914–2926. <https://doi.org/10.1016/J.RSE.2008.02.010>.
- Massey, R., Sankey, T.T., Yadav, K., Congalton, R.G., Tilton, J.C., Thenkabail, P.S., 2017. NASA Making Earth System Data Records for Use in Research Environments (MEaSUREs) Global Food Security-support Analysis Data (GFSAD) @ 30m for North America: Cropland Extent Product (GFSAD30NACE). NASA EOSDIS Land Processes DAAC. [https://doi.org/10.5067/MEAASURE/GFSAD/GFSAD30NACE.001](https://doi.org/10.5067/MEASURE/GFSAD/GFSAD30NACE.001).

- Meigs, G.W., Kennedy, R.E., Cohen, W.B., 2011. A Landsat time series approach to characterize bark beetle and defoliator impacts on tree mortality and surface fuels in conifer forests. *Remote Sens. Environ.* 115, 3707–3718. <https://doi.org/10.1016/J.RSE.2011.09.009>.
- Miller, J.D., Thode, A.E., 2007. Quantifying burn severity in a heterogeneous landscape with a relative version of the delta Normalized Burn Ratio (dNBR). *Remote Sens. Environ.* 109, 66–80. <https://doi.org/10.1016/J.RSE.2006.12.006>.
- Natural Resources Canada, Canadian Forest Service, Ottawa, 2017. The State of Canada's Forests. Annual Report 2017. Available from: <https://cfs.nrcan.gc.ca/publications?id=38871> (accessed on 11 Feb 2021).
- Olofsson, P., Foody, G.M., Herold, M., Stehman, S.V., Woodcock, C.E., Wulder, M.A., 2014. Good practices for estimating area and assessing accuracy of land change. *Remote Sens. Environ.* 148, 42–57. <https://doi.org/10.1016/j.rse.2014.02.015>.
- Olofsson, P., Arévalo, P., Espejo, A.B., Green, C., Lindquist, E., McRoberts, R.E., Sanz, M.J., 2020. Mitigating the effects of omission errors on area and area change estimates. *Remote Sens. Environ.* 236, 111492 <https://doi.org/10.1016/j.rse.2019.111492>.
- Overpeck, J.T., Rind, D., Goldberg, R., 1990. Climate-induced changes in forest disturbance and vegetation. *Nature* 343, 51–53. <https://doi.org/10.1038/343051a0>.
- Pasquarella, V.J., Bradley, B.A., Woodcock, C.E., 2017. Near-real-time monitoring of insect defoliation using Landsat time series. *Forests* 8. <https://doi.org/10.3390/f8080275>.
- Pasquarella, V.J., Holden, C.E., Woodcock, C.E., 2018. Improved mapping of forest type using spectral-temporal Landsat features. *Remote Sens. Environ.* 210, 193–207. <https://doi.org/10.1016/J.RSE.2018.02.064>.
- Price, D.T., Alfaro, R.I., Brown, K.J., Flannigan, M.D., Fleming, R.A., Hogg, E.H., Girardin, M.P., Lakusta, T., Johnston, M., McKenney, D.W., Pedlar, J.H., Stratton, T., Sturrock, R.N., Thompson, I.D., Trofymow, J.A., Venier, L.A., 2013. Anticipating the consequences of climate change for Canada's boreal forest ecosystems1. *Environ. Rev.* <https://doi.org/10.1139/er-2013-0042>.
- Schroeder, T.A., Healey, S.P., Moisen, G.G., Frescino, T.S., Cohen, W.B., Huang, C., Kennedy, R.E., Yang, Z., 2014. Improving estimates of forest disturbance by combining observations from Landsat time series with U.S. Forest Service Forest Inventory and Analysis data. *Remote Sens. Environ.* 154, 61–73. <https://doi.org/10.1016/J.RSE.2014.08.005>.
- Schroeder, T.A., Schleeweis, K.G., Moisen, G.G., Toney, C., Cohen, W.B., Freeman, E.A., Yang, Z., Huang, C., 2017. Testing a Landsat-based approach for mapping disturbance causality in U.S. forests. *Remote Sens. Environ.* 195, 230–243. <https://doi.org/10.1016/j.rse.2017.03.033>.
- Seidl, R., Thom, D., Kautz, M., Martin-Benito, D., Peltoniemi, M., Vacchiano, G., Wild, J., Ascoli, D., Petr, M., Honkanием, J., Lexer, M.J., Trotsiuk, V., Mairota, P., Svoboda, M., Fabrika, M., Nagel, T.A., Reyer, C.P.O., 2017. Forest disturbances under climate change. *Nat. Clim. Chang.* 7, 395–402. <https://doi.org/10.1038/nclimate3303>.
- Senf, C., Seidl, R., 2021. Mapping the forest disturbance regimes of Europe. *Nat. Sustain.* 4, 63–70. <https://doi.org/10.1038/s41893-020-00609-y>.
- Senf, C., Pflugmacher, D., Hostert, P., Seidl, R., 2017a. Using Landsat time series for characterizing forest disturbance dynamics in the coupled human and natural systems of Central Europe. *ISPRS J. Photogramm. Remote Sens.* 130, 453–463. <https://doi.org/10.1016/j.isprsjprs.2017.07.004>.
- Senf, C., Seidl, R., Hostert, P., 2017b. Remote sensing of forest insect disturbances: current state and future directions. *Int. J. Appl. Earth Obs. Geoinf.* <https://doi.org/10.1016/j.jag.2017.04.004>.
- Song, X.-P., Hansen, M.C., Stehman, S.V., Potapov, P.V., Tyukavina, A., Vermote, E.F., Townshend, J.R., 2018. Global land change from 1982 to 2016. *Nature*. <https://doi.org/10.1038/s41586-018-0411-9>.
- Soverel, N.O., Perrakis, D.D.B., Coops, N.C., 2010. Estimating burn severity from Landsat dNBR and RdNBR indices across western Canada. *Remote Sens. Environ.* 114, 1896–1909. <https://doi.org/10.1016/j.rse.2010.03.013>.
- Stehman, S.V., 2014. Estimating area and map accuracy for stratified random sampling when the strata are different from the map classes. *Int. J. Remote Sens.* 35, 4923–4939. <https://doi.org/10.1080/01433161.2014.930207>.
- Stehman, S.V., Foody, G.M., 2019. Key issues in rigorous accuracy assessment of land cover products. *Remote Sens. Environ.* <https://doi.org/10.1016/j.rse.2019.05.018>.
- Sulla-Menashe, D., Friedl, M.A., Woodcock, C.E., 2016. Sources of bias and variability in long-term Landsat time series over Canadian boreal forests. *Remote Sens. Environ.* 177, 206–219. <https://doi.org/10.1016/J.RSE.2016.02.041>.
- Sulla-Menashe, D., Woodcock, C.E., Friedl, M.A., 2018. Canadian boreal forest greening and browning trends: an analysis of biogeographic patterns and the relative roles of disturbance versus climate drivers. *Environ. Res. Lett.* 13, 014007 <https://doi.org/10.1088/1748-9326/aa9b88>.
- Swann, A.L., Fung, I.Y., Levis, S., Bonan, G.B., Doney, S.C., 2010. Changes in Arctic vegetation amplify high-latitude warming through the greenhouse effect. *Proc. Natl. Acad. Sci. U. S. A.* 107, 1295–1300. <https://doi.org/10.1073/pnas.0913846107>.
- Tang, X., Bullock, E.L., Olofsson, P., Estel, S., Woodcock, C.E., 2019. Near real-time monitoring of tropical forest disturbance: new algorithms and assessment framework. *Remote Sens. Environ.* 224, 202–218. <https://doi.org/10.1016/J.RSE.2019.02.003>.
- The government of British Columbia, 2021. Aerial Overview Surveys. <https://www2.gov.bc.ca/gov/content/industry/forestry/managing-our-forest-resources/forest-health/aerial-overview-surveys>.
- Trenberth, K.E., Hoar, T.J., 1996. The 1990–1995 El Niño–Southern oscillation event: longest on record. *Geophys. Res. Lett.* 23, 57–60. <https://doi.org/10.1029/95GL03602>.
- Tucker, C.J., 1979. Red and photographic infrared linear combinations for monitoring vegetation. *Remote Sens. Environ.* 8 (2), 127–150.
- Turner, D.P., Ritts, W.D., Kennedy, R.E., Gray, A.N., Yang, Z., 2015. Effects of harvest, fire, and pest/pathogen disturbances on the West Cascades ecoregion carbon balance. *Carbon Balance Manag.* 10. <https://doi.org/10.1186/s13021-015-0022-9>.
- Tyukavina, A., Stehman, S.V., Potapov, P.V., Turubanova, S.A., Baccini, A., Goetz, S.J., Laporte, N.T., Houghton, R.A., Hansen, M.C., 2013. National-scale estimation of gross forest aboveground carbon loss: a case study of the Democratic Republic of the Congo. *Environ. Res. Lett.* 8, 044039 <https://doi.org/10.1088/1748-9326/8/4/044039>.
- Tyukavina, A., Baccini, A., Hansen, M.C., Potapov, P.V., Stehman, S.V., Houghton, R.A., Krylov, A.M., Turubanova, S., Goetz, S.J., 2015. Aboveground carbon loss in natural and managed tropical forests from 2000 to 2012. *Environ. Res. Lett.* 10, 074002 <https://doi.org/10.1088/1748-9326/10/7/074002>.
- Tyukavina, A., Hansen, M.C., Potapov, P.V., Stehman, S.V., Smith-Rodriguez, K., Okpa, C., Aguilar, R., 2017. Types and rates of forest disturbance in Brazilian Legal Amazon, 2000–2013. *Sci. Adv.* 3, e1601047 <https://doi.org/10.1126/sciadv.1601047>.
- United States Department of Agriculture, 2009. Forest Service Common Trees of Alaska. Available from: https://www.fs.usda.gov/Internet/FSE_DOCUMENTS/stelprdb33_20147.pdf (accessed on 22 Mar 2021).
- Verbesselt, J., Hyndman, R., Newnham, G., Culvenor, D., 2010. Detecting trend and seasonal changes in satellite image time series. *Remote Sens. Environ.* 114, 106–115. <https://doi.org/10.1016/j.rse.2009.08.014>.
- Wang, J.A., Sulla-Menashe, D., Woodcock, C.E., Sonnentag, O., Keeling, R.F., Friedl, M.A., 2020. Extensive land cover change across Arctic–Boreal Northwestern North America from disturbance and climate forcing. *Glob. Chang. Biol.* <https://doi.org/10.1111/gcb.14804>.
- White, J.C., Wulder, M.A., Hermosilla, T., Coops, N.C., Hobart, G.W., 2017. A nationwide annual characterization of 25 years of forest disturbance and recovery for Canada using Landsat time series. *Remote Sens. Environ.* 194, 303–321. <https://doi.org/10.1016/j.rse.2017.03.035>.
- Wickham, J., Stehman, S.V., Gass, L., Dewitz, J.A., Sorenson, D.G., Granneman, B.J., Poss, R.V., Baer, L.A., 2017. Thematic accuracy assessment of the 2011 National Land Cover Database (NLCD). *Remote Sens. Environ.* 191, 328–341. <https://doi.org/10.1016/j.rse.2016.12.026>.
- Woodcock, C.E., Allen, R., Anderson, M., Belward, A., Bindschadler, R., Cohen, W., Gao, F., Goward, S.N., Helder, D., Helmer, E., Nemani, R., Oreopoulos, L., Schott, J., Thenkabail, P.S., Vermote, E.F., Vogelmann, J., Wulder, M.A., Wynne, R., 2008. Free access to Landsat imagery. *Science* 320, 1011. <https://doi.org/10.1126/science.320.5879.1011a>.
- Woodcock, C.E., Loveland, T.R., Herold, M., Bauer, M.E., 2020. Transitioning from change detection to monitoring with remote sensing: a paradigm shift. *Remote Sens. Environ.* 238, 111558 <https://doi.org/10.1016/j.rse.2019.111558>.
- Wulder, M.A., Kurz, W.A., Gillis, M., 2004. National level forest monitoring and modeling in Canada. *Prog. Plan.* 61, 365–381.
- Wulder, M.A., Masek, J.G., Cohen, W.B., Loveland, T.R., Woodcock, C.E., 2012. Opening the archive: how free data has enabled the science and monitoring promise of Landsat. *Remote Sens. Environ.* 122, 2–10. <https://doi.org/10.1016/j.rse.2012.01.010>.
- Yin, H., Prishchepov, A.V., Kuemmerle, T., Bleyhl, B., Buchner, J., Radloff, V.C., 2018. Mapping agricultural land abandonment from spatial and temporal segmentation of Landsat time series. *Remote Sens. Environ.* 210, 12–24. <https://doi.org/10.1016/j.rse.2018.02.050>.
- Zhao, F., Huang, C., Zhu, Z., 2015. Use of vegetation change tracker and support vector machine to map disturbance types in greater yellowstone ecosystems in a 1984–2010 landsat time series. *IEEE Geosci. Remote Sens. Lett.* 12, 1650–1654. <https://doi.org/10.1109/LGRS.2015.2418159>.
- Zhu, Z., 2017. Change detection using landsat time series: a review of frequencies, preprocessing, algorithms, and applications. *ISPRS J. Photogramm. Remote Sens.* <https://doi.org/10.1016/j.isprsjprs.2017.06.013>.
- Zhu, Z., Woodcock, C.E., 2014a. Continuous change detection and classification of land cover using all available Landsat data. *Remote Sens. Environ.* 144, 152–171. <https://doi.org/10.1016/j.rse.2014.01.011>.
- Zhu, Z., Woodcock, C.E., 2014b. Automated cloud, cloud shadow, and snow detection in multitemporal Landsat data: an algorithm designed specifically for monitoring land cover change. *Remote Sens. Environ.* 152, 217–234. <https://doi.org/10.1016/j.rse.2014.06.012>.
- Zhu, Z., Woodcock, C.E., Holden, C., Yang, Z., 2015. Generating synthetic Landsat images based on all available Landsat data: predicting Landsat surface reflectance at any given time. *Remote Sens. Environ.* 162, 67–83. <https://doi.org/10.1016/j.rse.2015.02.009>.